

## Role of the Secondary Coordination Sphere in Metal-Mediated Dioxygen Activation

Ryan L. Shook and A. S. Borovik\*

*Department of Chemistry, University of California—Irvine, 1102 Natural Sciences II, Irvine, California 92697-2025*

Received August 4, 2009

Alfred Werner proposed nearly 100 years ago that the secondary coordination sphere has a role in determining the physical properties of transition-metal complexes. We now know that the secondary coordination sphere impacts nearly all aspects of transition-metal chemistry, including the reactivity and selectivity in metal-mediated processes. These features are highlighted in the binding and activation of dioxygen by transition-metal complexes. There are clear connections between control of the secondary coordination sphere and the ability of metal complexes to (1) reversibly bind dioxygen or (2) bind and activate dioxygen to form highly reactive metal–oxo complexes. In this Forum Article, several biological and synthetic examples are presented and discussed in terms of structure–function relationships. Particular emphasis is given to systems with defined noncovalent interactions, such as intramolecular H-bonds involving dioxygen-derived ligands. To further illustrate these effects, the homolytic cleavage of C–H bonds by metal–oxo complexes with basic oxo ligands is described.

### Introduction

In 1912, Alfred Werner advanced the idea that micro-environments surrounding transition-metal complexes affect the structure and function.<sup>1,2</sup> This new idea invoked the concept that metal complexes can interact with other molecules in specific ways, forming secondary-sphere (or outer-sphere) species. Until that time, molecular chemistry had developed along the line that the primary coordination sphere was the only contributor to the properties of metal complexes. It is true that essential properties of metal complexes are linked to the primary coordination sphere; however, that alone was not sufficient to explain all of Werner's experimental findings. For instance, the secondary coordination sphere effects were needed in order to explain the association of amines with coordinatively saturated  $[M(\text{acac})_3]^n$  complexes and the presence of solvent molecules in crystals of metal complexes. Werner was unaware of the chemical forces acting within the secondary coordination sphere and how they could be utilized to direct chemistry.

Since Werner's seminal insights, the effects of both the primary and secondary coordination spheres have been probed by numerous spectroscopic, analytical, theoretical, and kinetic methods. Fundamental differences are now known to exist between the two coordination spheres and can be understood within the context of chemical bonding.

The primary coordination sphere is dominated by covalent interactions between donor atoms on ligands and metal ions. Experimental and theoretical investigations have provided detailed structure–function relationships that have improved the understanding of key properties, such as correlations between electronic and molecular structures and chemical reactivity, and the development of organometallic catalysts. In contrast, the secondary coordination sphere normally utilizes noncovalent interactions and is associated with determining chemical selectivity.

The growing body of evidence has clearly indicated that control of both spheres is necessary to achieve highly functional complexes. Yet, few synthetic systems regulate both the primary and secondary coordination spheres in a predictable manner. The scarcity of such systems can be linked in large part to the secondary coordination sphere and the inability to utilize noncovalent interactions in a reliable and reproducible manner. Because noncovalent bonds are generally weak interactions, they tend to be difficult to control within the secondary coordination sphere, leading to the formation of various structures and perturbation of function. These difficulties have led to noncovalent interactions being often overlooked in the design of metal complexes and being relegated to solvation phenomena.<sup>2</sup>

Our thinking about the influences *and usefulness* of the secondary coordination sphere changed with the advent of host–guest chemistry and the emergence of structural metallobiochemistry. The idea that metal complexes could be “recognized” by other molecules via binding to the coordinated ligands (and not the metal centers) was found soon after the realization that host compounds, such as

\*To whom correspondence should be addressed. E-mail: aborovik@uci.edu.  
(1) (a) Werner, A. *Ann Chem.* 1912, 386, 1–272. (b) Werner, A. *Ber. Dtsch. Chem. Ges.* 1912, 45, 121–130.  
(2) Colquhoun, H. M.; Stoddart, J. F.; Williams, D. J. *Angew. Chem., Int. Ed. Engl.* 1986, 25, 487–507.

crown ethers, cavitands, and cyptands, could bind anions and small molecules.<sup>3</sup> These findings led to several reports of secondary sphere coordination complexes, examples of which are species formed with crown ethers and metal complexes containing ammine or aquo ligands (Figure 1).<sup>4,5</sup> Note that the *intermolecular* forces used to form these host–guest species are hydrogen bonds (H bonds).

The breakthrough in spectroscopic and X-ray diffraction (XRD) analyses of metalloproteins is arguably the most important advance in understanding how to integrate the primary and secondary coordination spheres in inorganic chemistry. Information obtained from these studies illustrate in striking clarity that control of both the primary and secondary coordination spheres can be accomplished in an *intramolecular* manner. Protein active sites have numerous architectural features that aid in regulating function, including (1) metal binding sites utilizing endogenous ligands from amino acid side chains to regulate the primary coordination spheres, (2) site isolation (when necessary) to avoid unwanted metal ion–metal ion interactions, (3) channels or paths to allow external reagents access to the functionally vital metal center(s), and (4) control of the secondary coordination sphere through protein-derived architectures. These findings have challenged chemists to design and prepare synthetic systems that control both the primary and secondary coordination spheres. This Forum Article describes some of the biological and synthetic systems that utilize simultaneous regulation of both spheres to achieve dioxygen binding and activation. In particular, we will examine how intramolecular H bonds in the secondary coordination sphere affect function. Correlations between structure and function will be highlighted, with emphasis on the benefits in regulating the secondary coordination sphere during dioxygen activation.

### The Problem: Preventing Unwanted Multimetallic Species

Although thermodynamically favorable, dioxygen needs to be associated with other species for O–O bond cleavage to occur. The association with other species is a kinetic necessity in order to overcome barriers arising from dioxygen's triplet ground state. Metal complexes have many of the requisite properties to bind and activate dioxygen and thus have been utilized by biological and synthetic systems. The normal binding of dioxygen involves electron transfer from the metal center(s) to the dioxygen, forming metal–superoxo or –peroxo species. The reduction of dioxygen leads to difficulties for any subsequent chemistry involving metal–O<sub>2</sub> complexes, the most frequent being O–O bond cleavage and the formation of metal oxide compounds. For instance, monomeric M–O<sub>2</sub> complexes (M = Cu, Fe, and Mn) are rare because of the thermodynamic propensity to form multimetallic complexes containing oxo- and hydroxo-bridged complexes (Figure 2).<sup>6</sup> These species are often

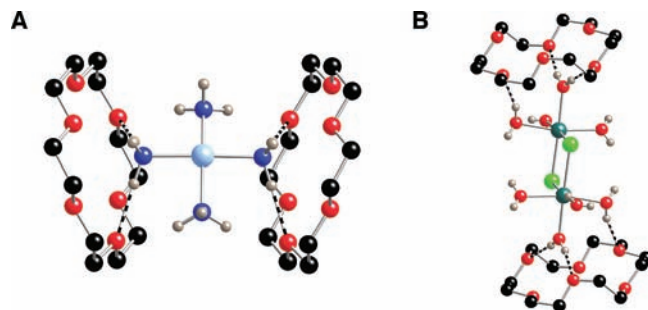


**Figure 1.** Two examples of secondary coordination sphere interactions within crystalline lattices: (A) 18-crown-6·[Cu<sup>II</sup>(NH<sub>3</sub>)<sub>4</sub>] and (B) 18-crown-6·[Mn<sup>II</sup>(H<sub>2</sub>O)<sub>4</sub>(Cl)<sub>2</sub>]. Only ammine and aquo H atoms are shown for clarity.

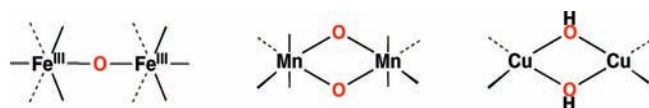


**Figure 2.** Common structural motifs that arise from the activation of dioxygen by iron, manganese, and copper complexes.

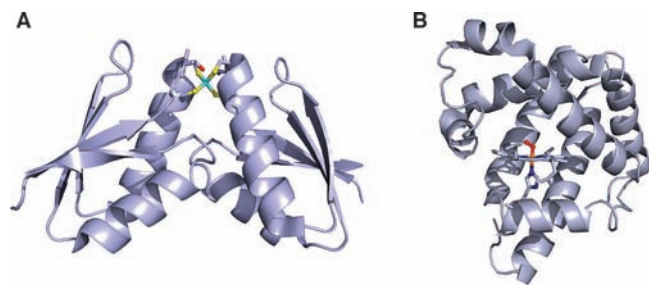


**Figure 3.** Molecular structures of the homodimeric copper-trafficking protein Cu(Hah)<sub>2</sub> (PDB, 1FEE) (A) and myoglobin (PDB, 1A6M) (B).

exceedingly stable and do not function as either O<sub>2</sub> carriers or reagents to oxidize substrates.

**Site-Isolation Approach.** One means to circumvent the formation of these unwanted oxo/hydroxo-bridged species is to physically isolate each metal center to such an extent that dimerization is prevented. Site isolation is best illustrated in the placement of active sites in metalloproteins. Comparisons of various molecular structures show correlations between function and the location of the active sites within the proteins. In general, the active sites in electron transfer and metallotrafficking proteins (Figure 3A) are found near the molecular surface, an obvious evolutionary benefit for these proteins because of their functional need for these active sites to closely interact with other species. In contrast, the dioxygen-binding proteins hemoglobin and myoglobin (Figure 3B) have active sites somewhat buried within the protein matrix, presumably, in part, to prevent unwanted metal–metal interactions with neighboring molecules. This is further demonstrated by the cytochrome P450 compounds, a family of monooxygenases with internal active sites.

Not surprisingly, there have been several efforts to design synthetic systems that incorporate site-isolation characteristics. However, few have been as successful as metalloproteins in the reversible binding of dioxygen or O<sub>2</sub> activation. This is especially true of iron, manganese,

(3) (a) Pederson, C. J. *Angew. Chem., Int. Ed. Engl.* **1988**, *27*, 1021–1027. (b) Cram, D. J. *Angew. Chem., Int. Ed. Engl.* **1988**, *27*, 1009–1020. (c) Lehn, J. M. *Angew. Chem., Int. Ed. Engl.* **1988**, *27*, 89–112.

(4) Colquhoun, H. M.; Stoddart, J. F.; Williams, D. K. *J. Chem. Soc., Chem. Commun.* **1981**, 849–850.

(5) Xianglin, J.; Zuohua, P.; Meicheng, S.; Youqi, T.; Depei, H.; Zihou, T.; Jinqi, Z. K. *Chin. Sci. Bull.* **1983**, *28*, 1334.

(6) (a) Kurtz, D. M. *Chem. Rev.* **1990**, *90*, 585–606. (b) Mirica, L. M.; Ottenwaelder, X.; Stack, T. D. P. *Chem. Rev.* **2004**, *104*, 1013–1046. (c) Lewis, E. A.; Tolman, W. B. *Chem. Rev.* **2004**, *104*, 1047–1076. (d) Wu, A. J.; Penner-Hahn, J. E.; Pecoraro, V. L. *Chem. Rev.* **2004**, *104*, 903–938.

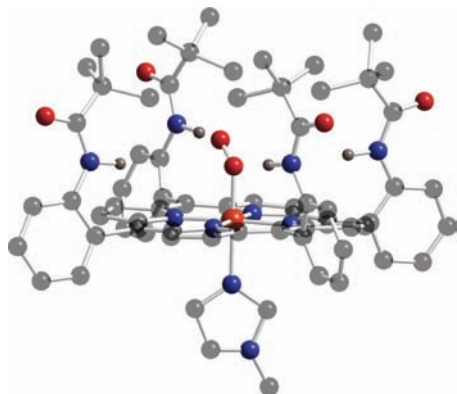


**Figure 4.** Molecular structure of the Fe–O<sub>2</sub> picket-fence porphyrin complex.

and copper complexes, in which dioxygen binding under ambient conditions ultimately leads to species with bridging cores (Figure 2). With this said, there have been some notable examples demonstrating that steric bulk within the secondary coordination sphere can produce important findings. Arguably, the best-known example of this approach is the ferrous “picket-fence” porphyrin complex of Collman (Figure 4).<sup>7</sup> The steric bulk in this system comes from four functionalized aryl groups attached at the meso positions of the porphyrin ring. One regioisomer has all of the bulky amide groups positioned on the same side of the ring, producing a sterically constrained cavity that is suitable for dioxygen binding. Efficient dioxygen binding requires a five-coordinate iron(II) center, which is accessible by binding of an imidazole ligand to the vacant site on the unhindered side of the complex. Importantly, the cavity is sufficiently confined to prevent the formation of six-coordinate, bis(imidazole) species. There is enough room to have smaller molecules, such as dioxygen, enter the cavity and bind to the iron center: there are several reports illustrating the reversible binding of dioxygen and other small molecules under ambient conditions. Over the years, Collman has used this system to explore the fundamental aspects of dioxygen binding and, more recently, elaborated on the design to investigate other multimetal enzymatic systems, including cytochrome *c* oxidase.<sup>8</sup>

Incorporating steric bulk into other ligand types has also been instrumental in obtaining stable dioxygen

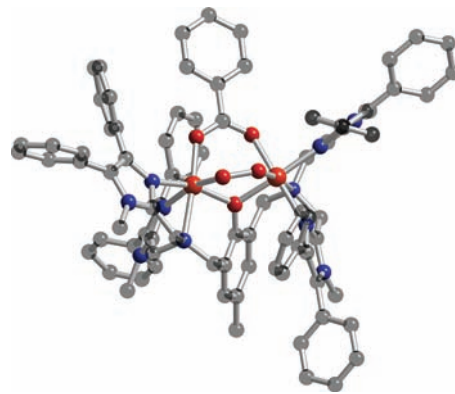


**Figure 5.** Molecular structure of a diiron–( $\mu$ -1,2-peroxo) complex containing a bulky binucleating ligand.

adducts of nonheme complexes. For nonheme iron complexes, only three diiron–( $\mu$ -1,2-peroxo) species have been stable enough to be structurally characterized: two of these are only isolable at temperatures below  $-20\text{ }^{\circ}\text{C}$ .<sup>9</sup> Suzuki developed the other complex using a hindered binucleating ligand containing several appended aryl groups (Figure 5).<sup>9d</sup> The diiron–( $\mu$ -1,2-peroxo) complex with this ligand is prepared at room temperature and reversibly binds dioxygen. An amazing aspect of this system was that removal of the dioxygen from the diiron–( $\mu$ -1,2-peroxo) complex was achieved in boiling acetonitrile, conditions expected to lead to irreversible oxidation to give oxo-bridged species. Two reasons, both involving the aryl groups, were postulated to account for the observed chemistry. First, the presence of two aryl rings on each imidazole moiety caused a weakening of the Fe–N bonds because of steric repulsions, which, in turn, affected the iron centers’ ability to further reduce the peroxo ligand. Second, the aryl rings created a sterically constrained hydrophobic cavity around the metal centers, which allowed entry of dioxygen but not other species, especially other diiron complexes that would lead to irreversible oxidation.

A similar use of sterically bulky groups was needed to control dioxygen binding in copper systems with Tp<sup>R,R'</sup> ligands [Tp = hydrotris(3,5-R,R'-pyrazolyl)borates]. Early work with [Cu<sup>I</sup>Tp<sup>Me,Me</sup>] systems gave some indications that a Cu–O<sub>2</sub> adduct could be stabilized, but the data were incomplete because of complications from competing side reactions.<sup>10</sup> Kitajima realized that changing the R groups to Tp<sup>tBu,iPr</sup> would provide enough steric limitation to isolate the first copper–superoxo complex (Figure 6A).<sup>11</sup> Moreover, a change to isopropyl groups at the 3 position of the pyrazole rings led to a relatively stable dimeric copper–peroxo complex, with a  $\mu$ - $\eta^2$ : $\eta^2$ -peroxodicopper(II) core (Figure 6B).<sup>12</sup> Even though the isopropyl groups did not directly interact with the  $\mu$ - $\eta^2$ : $\eta^2$ -peroxodicopper(II) core, their presence was clearly important by permitting dimerization but limiting other intermolecular oxidative processes.

(7) (a) Jameson, G. B.; Molinaro, F. S.; Ibers, J. A.; Collman, J. P.; Brauman, J. I.; Rose, E.; Suslick, K. S. *J. Am. Chem. Soc.* **1978**, *100*, 6769–6770. (b) Collman, J. P.; Brauman, J. I.; Doxsee, K. M.; Halbert, T. R.; Bunnenberg, E.; Linder, R. E.; LaMar, G. N.; Del Gaudio, J.; Lang, G.; Spartalian, K. *J. Am. Chem. Soc.* **1980**, *102*, 4182–4192. (c) Collman, J. P.; Brauman, J. I.; Iverson, B. L.; Sessler, J. L.; Morris, R. M.; Gibson, Q. H. *J. Am. Chem. Soc.* **1983**, *105*, 3052–3064. (d) Collman, J. P.; Zhang, Z.; Wong, K.; Brauman, J. I. *J. Am. Chem. Soc.* **1994**, *116*, 6245–6251. (e) Momenteau, M.; Reed, C. A. *Chem. Rev.* **1994**, *94*, 659–698.

(8) Collman, J. P.; Boulatov, R.; Sunderland, C. J.; Fu, L. *Chem. Rev.* **2004**, *104*, 561–588.

(9) (a) Dong, Y.; Yan, S.; Young, V. G., Jr.; Que, L., Jr. *Angew. Chem., Int. Ed. Engl.* **1996**, *108*, 618–620. (b) Kitajima, N.; Tamura, N.; Amagai, H.; Fukui, H.; Moro-oka, Y.; Mizutani, Y.; Kitagawa, T.; Mathur, R.; Heerwegh, K.; Reed, C. A.; Randall, C. R.; Que, L., Jr.; Tatsumi, K. *J. Am. Chem. Soc.* **1994**, *116*, 9071–9085. (c) Kim, K.; Lippard, S. J. *J. Am. Chem. Soc.* **1996**, *118*, 4914–4915. (d) Ookubo, T.; Sugimoto, H.; Nagayama, T.; Masuda, H.; Sato, T.; Tanaka, Y.; Maeda, Y.; Okawa, H.; Hayashi, Y.; Uehara, A.; Suzuki, M. *J. Am. Chem. Soc.* **1996**, *118*, 701–702.

(10) Thompson, J. S. *J. Am. Chem. Soc.* **1984**, *106*, 4057–4058.

(11) Fujisawa, K.; Tanaka, M.; Moro-oka, Y.; Kitajima, N. *J. Am. Chem. Soc.* **1994**, *116*, 12079–12080.

(12) (a) Kitajima, N.; Fujisawa, K.; Moro-oka, Y. *J. Am. Chem. Soc.* **1989**, *111*, 8975–8976. (b) Kitajima, N.; Fujisawa, K.; Fujimoto, C.; Moro-oka, Y.; Hashimoto, S.; Kitagawa, T.; Toriumi, K.; Tatsumi, K.; Nakamura, A. *J. Am. Chem. Soc.* **1992**, *114*, 1277–1291.

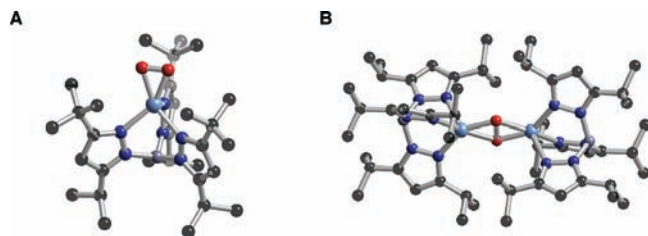


**Figure 6.** Molecular structures of copper–superoxo complex  $[\text{CuTp}^{\text{t-Bu,Pr}}(\eta^2\text{-O}_2)]$  (A) and  $\mu\text{-}\eta^2\text{:}\eta^2\text{-peroxodicopper(II)}$  complex  $[\text{Cu}^{\text{II}}\text{Tp}^{\text{tPr,iPr}}]_2(\text{O}_2)$  (B) showing the controlling effects of steric bulk.

Note that this  $\eta^2\text{:}\eta^2\text{-peroxodicopper(II)}$  complex was a landmark discovery in synthetic bioinorganic chemistry because it correctly predicted the active-site structure of the oxygenated form of the respiratory protein hemocyanin. Furthermore, this series of copper complexes provides an excellent illustration of how incremental adjustments within the secondary coordination sphere can have a major impact on functional aspects of dioxygen binding to transition-metal complexes.

More recently, bulkier ligand systems have been employed to create larger cavities around metal centers for dioxygen binding. Notable examples are the calix[6]arene ligands of Renaud, which contain various tripodal ligands for the binding of a single metal ion. Application of these systems toward dioxygen activation by copper complexes has been reported.<sup>13</sup>

### H-Bonding Networks

**Metalloproteins.** Further control of the binding and activation of dioxygen is possible through the use of H bonds within the secondary coordination sphere. Examples of this approach using *intermolecular* H bonds have already been discussed in connection with the host–guest chemistry. *Intramolecular* H bonds are now recognized to also be extremely important in controlling chemistry occurring at metal centers. Thus, coupling of the effects of site isolation and the H-bonding network, both within the secondary coordination sphere, can be used to impact metal-mediated transformations.

The best examples of intramolecular H-bonding networks are from biomolecules. H bonds have bond strengths ranging from 5 to 15 kcal/mol in the condensed phase, which are generally much weaker than covalent interactions found within the primary spheres.<sup>14</sup> Even though H bonds are weak interactions, they are essential for the binding of dioxygen in hemoglobins and myoglobins. As depicted in Figure 7A with human hemoglobin, dioxygen binds to the iron centers in these proteins via a covalent Fe–O bond and a H bond between the distal

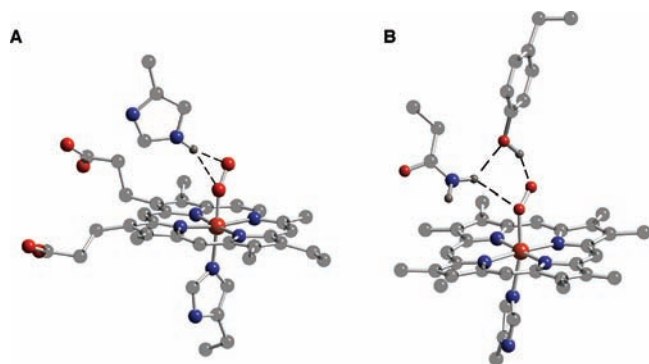


**Figure 7.** Active-site structures of the oxygenated forms of human hemoglobin (A) and nematode hemoglobin (B) illustrating the different H-bonding networks.

imidazolyl residue of histidine and the coordinated dioxygen.<sup>15,16</sup> Altering the position of the distal histidine in these proteins has pronounced functional effects, an example of which is the enhanced peroxidase activity observed for myoglobins, whose active sites have been engineered to eliminate bifurcated H-bond formation.<sup>17</sup> Moreover, changes in the H-bonding network can influence the O<sub>2</sub> affinity, as found when comparing the hemoglobins from human and parasitic nematode *Ascaris suum* (Figure 7B).<sup>18</sup> Nematodes normally exist in environments having low dioxygen concentrations, especially when compared to those experienced by humans. Notice that the primary coordination spheres around the iron centers are identical in the two hemoglobins. However, their H-bonding networks differ, which appears to affect the dioxygen binding, causing the nematode hemoglobin to have 10<sup>4</sup> times greater affinity for O<sub>2</sub>.

Hydrogen bonds formed within the secondary coordination sphere also influence dioxygen activation in a number of iron–heme enzymes. For instance, the function of cytochrome P450 compounds, heme-containing monooxygenases that are ubiquitous in nature, has been linked with a protein-derived H-bonding network within the secondary coordination sphere of the iron center (*vide infra*).<sup>19</sup> In addition, recent structural studies have implicated active-site H-bonding networks in the function of nonheme halogenases.<sup>20</sup> SyrB2, a nonheme iron(II)/ $\alpha$ -ketoglutarate ( $\alpha$ KG)-dependent halogenase, catalyzes the conversion of L-Thr to 4-Cl-L-Thr, a modification that is essential for the antifungal activity of syringomycin E.<sup>21</sup> The proposed mechanism involves Cl<sup>−</sup>,

(13) (a) Blanchard, S.; Le Clainche, L.; Rager, M.-N.; Chansou, B.; Tuchagues, J. P.; Duprat, A.; Le Mest, Y.; Renaud, O. *Angew. Chem., Int. Ed.* **1998**, *37*, 2732–2735. (b) Rondelez, Y.; Sènèque, O.; Rager, M.-N.; Duprat, A. F.; Renaud, O. *Chem.—Eur. J.* **2000**, *6*, 4218–4226. (c) Izzet, G.; Douzich, B.; Prangé, T.; Tomas, A.; Jabin, I.; Le Mest, Y.; Renaud, O. *Proc. Natl. Acad. Sci. U.S.A.* **2005**, *102*, 6831–6836. (d) Izzet, G.; Zeitouny, J.; Akdas-Killig, H.; Frapart, Y.; Menage, S.; Douzich, B.; Jabin, I.; Le Mest, Y.; Renaud, O. *J. Am. Chem. Soc.* **2008**, *130*, 9514–9523.

(14) (a) Elmsley, J. *Chem. Soc. Rev.* **1980**, *9*, 91–124. (b) Etter, M. C. *Acc. Chem. Res.* **1990**, *23*, 120–126.

(15) (a) Perutz, M. F.; Fermi, G.; Luisi, B.; Shaanan, B.; Liddington, R. C. *Acc. Chem. Res.* **1987**, *20*, 309–321. (b) Springer, B. A.; Sligar, S. G.; Olsen, J. S.; Philips, G. N., Jr. *Chem. Rev.* **1994**, *94*, 699–714.

(16) (a) Shaanan, B. *Nature* **1982**, *296*, 683–684. (b) Condon, P. J.; Royer, W. E., Jr. *J. Biol. Chem.* **1994**, *269*, 25259–25267. (c) Philips, S. E. V.; Schoenborn, B. P. *Nature* **1981**, *292*, 81–82.

(17) Ozaki, S.; Roach, M. P.; Matsui, T.; Watanabe, Y. *Acc. Chem. Res.* **2001**, *34*, 818–825.

(18) Yang, J.; Kloek, a. P.; Goldberg, D. E.; Matthews, F. S. *Proc. Natl. Acad. Sci. U.S.A.* **1995**, *92*, 4224–4228.

(19) (a) Martinis, S. A.; Atkins, W. M.; Stayton, P. S.; Sligar, S. G. *J. Am. Chem. Soc.* **1989**, *111*, 9252–9253. (b) Gerber, N. C.; Sligar, S. G. *J. Am. Chem. Soc.* **1992**, *114*, 8742–8743. (c) Schlichting, I.; Berendzen, J.; Chu, K.; Stock, A. M.; Maves, S. A.; Benson, D. E.; Sweet, R. M.; Ringe, D.; Pestko, G. A.; Sligar, S. G. *Science* **2000**, *287*, 1615–1622.

(20) For recent reviews on halogenases, see: (a) Vaillancourt, F. H.; Yeh, E.; Vosburg, D. A.; Garneau-Tsodikova, S.; Walsh, C. T. *Chem. Rev.* **2006**, *106*, 3364–3378. (b) Blasiak, L. C.; Drennan, C. L. *Acc. Chem. Res.* **2008**, *42*, 147–155.

(21) Vaillancourt, F. H.; Yin, J.; Walsh, C. T. *Proc. Natl. Acad. Sci. U.S.A.* **2005**, *102*, 10111–10116.

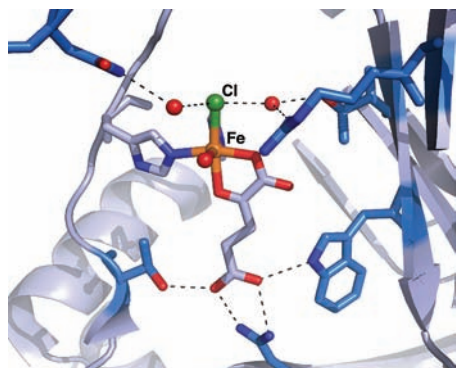


**Figure 8.** Active-site structure of SyrB2 showing the hydrogen-bonding network surrounding the  $\text{Cl}^-$  ion. The red spheres represent water molecules.

$\alpha\text{KG}$ , and  $\text{O}_2$  and proceeds through a  $[(\text{Cl})\text{Fe}^{\text{IV}}=\text{O}]$  intermediate (Figure 8). XRD studies on the reduced form of SyrB2 revealed that  $\text{Cl}^-$  is coordinated to the iron(II) center, replacing a carboxylate ligand that is normally found in this class of enzymes.<sup>22</sup> The  $\text{Fe}^{\text{II}}-\text{Cl}$  distance is unusually long at 2.44 Å,<sup>23</sup> in part because of two intramolecular H bonds involving  $\text{Cl}^-$  (Figure 8).<sup>24</sup> The functional consequences of these noncovalent interactions await further studies but may assist in the selective transfer of a Cl atom to the substrate.

**Synthetic Heme Systems.** Introducing similar hydrogen-bonding networks into synthetic systems has been challenging. Difficulties occur because of our inability to develop systems that are sufficiently rigid to promote intramolecular H-bond formation. The usual situations are that H-bond formation involving metal complexes occurs with other species present in the reaction mixture, leading to intermolecular products that do not have the chemical properties to promote the targeted function. To overcome this drawback, synthetic complexes must incorporate rigid frameworks that are positioned proximal to metal centers and contain H-bond donors or acceptors. These types of systems often require multistep syntheses that are difficult and time-intensive.

There have been some impressive examples of hydrogen-bonding networks within synthetic complexes. The H-bonding networks in hemoglobins and myoglobins have inspired investigations into the role of H bonds in binding dioxygen by synthetic heme complexes,<sup>25</sup> all of which contain H-bond donors appended from the meso positions of the porphyrin rings. Collman's picket-fence iron porphyrin is an example of such a system (Figure 4);<sup>26,27</sup> although placement of the amide groups is not within H-bonding distances, there appears to be a

dipole contribution that aids in the stabilization of the dioxygen adduct. The situation found with the picket-fence porphyrin complexes highlights a design problem with these systems for producing intramolecular H-bonding networks. The meso-C atoms are the most convenient positions to append H-bond donors/acceptors; however, attachment at these positions places functional groups too far from the metal center to engage in H bonds. To circumvent this problem, porphyrins have been designed to have rigid groups that “hang-over” the metal centers and thus bring H-bond donors/acceptors within critical distances to form intramolecular H bonds (Figure 9). Reed's urea/amide-appended porphyrins<sup>28</sup> and Chang's use of Kemp's acid-appended porphyrins are two of the most prominent examples of this approach.<sup>29</sup> Many of these models show a significant increase in affinity for dioxygen binding over comparable systems lacking H-bond donors. These results are consistent with the idea that intramolecular H bonds help to stabilize an  $\text{Fe}-\text{O}_2$  adduct. In addition, Nocera have prepared “Hangman” porphyrins that use xanthane units to position H-bond donors. In one example, they showed that a small network of H bonds is present around a  $\text{Fe}^{\text{III}}-\text{OH}$  unit, in both solution and the solid state (Figure 9C).<sup>30</sup>

**Other Synthetic Systems.** Nonheme systems have also been developed to incorporate functional groups that are capable of forming intramolecular H-bonding networks.<sup>31,32</sup> One of the first examples pertinent to dioxygen binding was reported by Kitajima, who isolated two isomers of a monomeric manganese(III)–peroxo complex that differ only by the absence or presence of an intramolecular H bond (Figure 10A).<sup>33</sup> Butler have reported an intriguing  $[\text{V}^{\text{V}}(\eta^2-\text{O}_2)(\text{O})]$  complex with a single intramolecular H bond (Figure 10B).<sup>34</sup> By far the most investigated nonheme systems are those containing tripodal ligands. Masuda et al. were the first to show the applicability of these systems using polypyridine tripods containing

(28) Wuenschell, G. E.; Tetreau, C.; Lavalette, D.; Reed, C. A. *J. Am. Chem. Soc.* **1992**, *114*, 3346–3355.

(29) Chang, C. K.; Liang, Y.; Avilés, G.; Peng, S.-M. *J. Am. Chem. Soc.* **1995**, *117*, 4191–4192.

(30) (a) Yeh, C.-Y.; Chang, C. J.; Nocera, D. G. *J. Am. Chem. Soc.* **2001**, *123*, 1513–1514. (b) Chang, L. L.; Chang, C. J.; Nocera, D. G. *Org. Lett.* **2003**, *5*, 2421–2424.

(31) (a) Mareques Rivas, J. C.; de Rosales, R. T. M.; Parsons, S. *Dalton Trans.* **2003**, 2156–2163. (b) Mareques Rivas, J. C.; Salvagni, E.; de Rosales, R. T. M.; Parsons, S. *Dalton Trans.* **2003**, 3339–3349. (c) Mareques Rivas, J. C.; Prabakaran, R.; de Rosales, R. T. M. *Chem. Commun.* **2004**, 76–77. (d) Mareques Rivas, J. C.; Salvagni, E.; Parsons, S. *Chem. Commun.* **2004**, 460–461. (e) Mareques Rivas, J. C.; de Rosales, R. T. M.; Parsons, S. *Chem. Commun.* **2004**, 610–611. (f) Mareques Rivas, J. C.; Prabakaran, R.; Parsons, S. *Dalton Trans.* **2004**, 1648–1655. (g) Mareques Rivas, J. C.; Prabakaran, R.; de Rosales, R. T. M.; Metteau, L.; Parsons, S. *Dalton Trans.* **2004**, 2800–2807. (h) Mareques Rivas, J. C.; Salvagni, E.; Parsons, S. *Dalton Trans.* **2004**, 4185–4192. (i) Feng, G.; Mareque-Rivas, J. C.; de Rosales, R. T. M.; Williams, N. H. *J. Am. Chem. Soc.* **2005**, *127*, 13470–13471. (j) Feng, G.; Mareque-Rivas, J. C.; Williams, N. H. *Chem. Commun.* **2006**, 1845–1847. (k) Mareque-Rivas, J. C.; Hinchley, S. L.; Metteau, L.; Parsons, S. *Dalton Trans.* **2006**, 2316–2322. (l) Metteau, L.; Parsons, S.; Mareque-Rivas, J. C. *Inorg. Chem.* **2006**, *45*, 6601–6603. (m) Feng, G.; Natale, D.; Prabakaran, R.; Mareque-Rivas, J. C.; Williams, N. H. *Angew. Chem., Int. Ed.* **2006**, *45*, 7056–7059.

(32) (a) Berreau, L. M.; Allred, R. A.; Makowski-Grzyska, M. M.; Arif, A. M. *Chem. Commun.* **2000**, 1423–1424. (b) Berreau, L. M.; Makowski-Grzyska, M. M.; Arif, A. M. *Inorg. Chem.* **2001**, *40*, 2212–2213.

(33) Kitajima, N.; Komatsuzaki, H.; Hikichi, S.; Osawa, M.; Moro-oka, Y. *J. Am. Chem. Soc.* **1994**, *116*, 11596–11597.

(34) Kinblin, C.; Bu, X.; Bulter, A. *Inorg. Chem.* **2002**, *41*, 158–160.

(22) Hegg, E. L.; Que, L., Jr. *Eur. J. Biochem.* **1997**, *250*, 625–629.

(23) Orpen, A. G.; Brammer, L.; Allen, F. H.; Kennard, O.; Watson, D. G.; Taylor, R. In *International Tables for Crystallography*; Wilson, A. J. C., Ed.; Kluwer Academic Publishers: Dordrecht, The Netherlands, 1995; Vol. C, pp 707–791.

(24) (a) Blasiak, L. C.; Vaillancourt, F. H.; Walsh, C.; Drennan, C. L. *Nature* **2006**, *440*, 368–371. (b) Wong, C.; Fujimoir, D. G.; Walsh, C. T.; Drennan, C. L. *J. Am. Chem. Soc.* **2009**, *131*, 4872–4879.

(25) Momenteau, M.; Reed, C. A. *Chem. Rev.* **1994**, *94*, 659–698 and references cited therein.

(26) (a) Collman, J. P. *Acc. Chem. Res.* **1977**, *10*, 265–272. (b) Jameson, G. B.; Drago, R. S. *J. Am. Chem. Soc.* **1985**, *107*, 3017–3022.

(27) Collman, J. P.; Zhang, X.; Wong, K.; Bauman, J. I. *J. Am. Chem. Soc.* **1994**, *116*, 6245–6251.

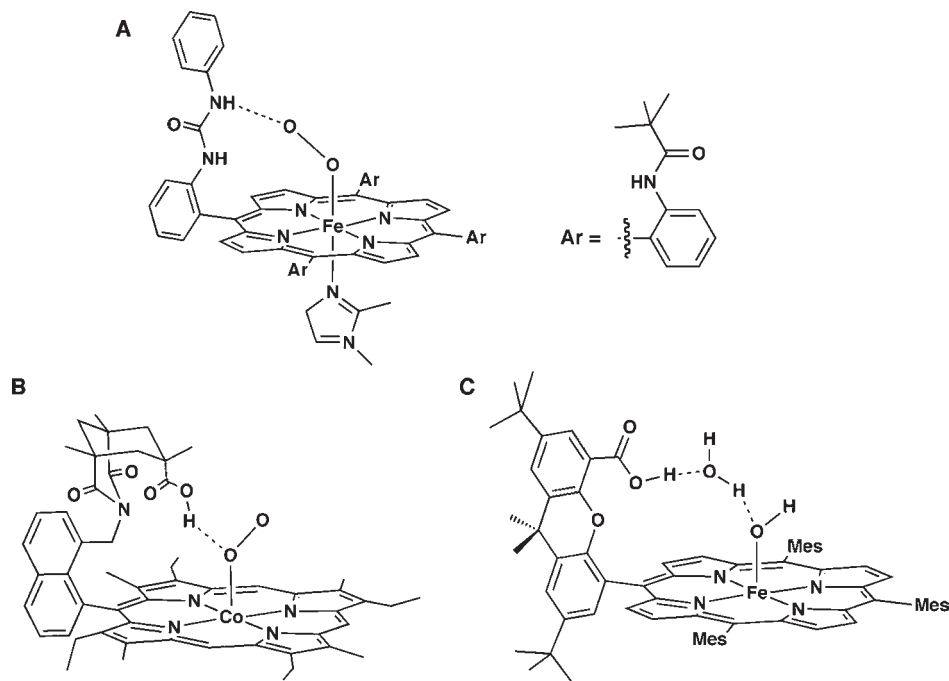


**Figure 9.** Hydrogen-bonding porphyrin systems: urea-modified “picket-fence” porphyrin (only the urea group is shown for clarity) (A),<sup>28</sup> system developed by Chang (B),<sup>29</sup> Fe<sup>III</sup>–OH “Hangman” porphyrin complex (C).<sup>30</sup>

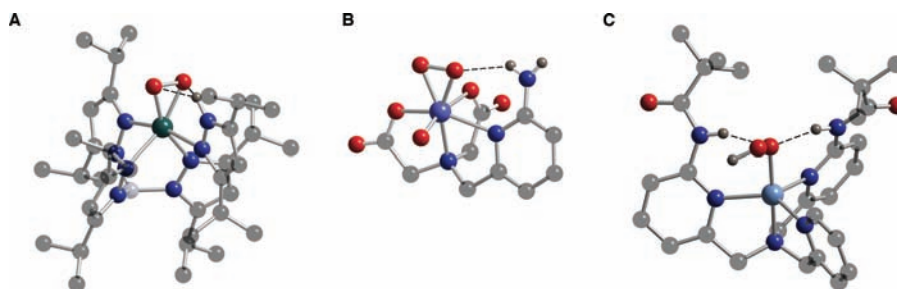
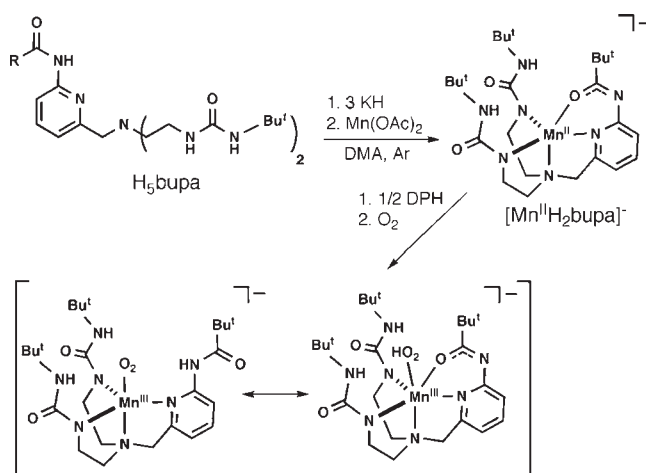


**Figure 10.** Molecular structures of metal–peroxo complexes with intramolecular H bonds: [Mn<sup>III</sup>(O<sub>2</sub>)] (A);<sup>33</sup> [V<sup>V</sup>(O<sub>2</sub>)(O)]<sup>-</sup> (B);<sup>34</sup> [Cu<sup>II</sup>(OOH)]<sup>+</sup> (C).<sup>35c</sup>

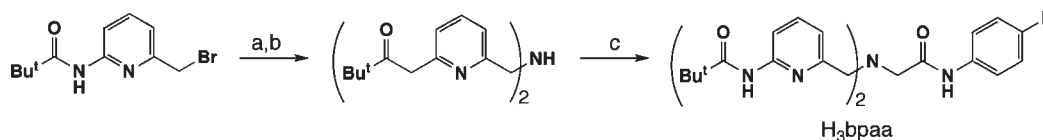
appended H-bond donors.<sup>35</sup> They have done extensive work in this field and have motivated many workers to explore the effects of intramolecular H-bonding networks. For instance, they developed a series of tris(carboxamidopyridyl) tripods, in which the hindered amide groups serve as H-bond donors. One of these ligands was used to isolate the first example of a stable Cu<sup>II</sup>–OOH complex, in which two intramolecular H bonds are formed between the ligand and proximal O atom of the hydroperoxide (Figure 10C).<sup>35c</sup> This complex was not generated from dioxygen, but rather it was formed using a copper(II) precursor complex and hydrogen peroxide. Nevertheless, it is an important contribution to copper–peroxo chemistry and illustrates the usefulness of intramolecular H-bonding networks.

(35) (a) Harata, M.; Jitsukawa, K.; Masuda, H.; Einaga, H. *Chem. Lett.* **1995**, *24*, 61–62. (b) Ogo, S.; Wada, S.; Watanabe, Y.; Iwase, M.; Wada, A.; Harata, M.; Jitsukawa, K.; Masuda, H.; Einaga, H. *Angew. Chem., Int. Ed.* **1998**, *37*, 2101–2104. (c) Wada, A.; Harata, M.; Hasegawa, K.; Jitsukawa, K.; Masuda, H.; Mukai, M.; Kitagawa, T.; Einaga, H. *Angew. Chem., Int. Ed.* **1998**, *37*, 798–799. (d) Ogo, S.; Yamahara, R.; Roach, M.; Suenobu, T.; Aki, M.; Ogura, T.; Kitagawa, T.; Masuda, H.; Fukuzumi, S.; Watanabe, Y. *Inorg. Chem.* **2002**, *41*, 5513–5520. (e) Yamaguchi, S.; Wada, A.; Funahashi, Y.; Nagatomo, S.; Kitagawa, T.; Jitsukawa, K.; Masuda, H. *Eur. J. Inorg. Chem.* **2003**, 4378–4386. (f) Wada, A.; Ogo, S.; Nagatomo, S.; Kitagawa, T.; Watanabe, Y.; Jitsukawa, K.; Masuda, H. *Inorg. Chem.* **2002**, *41*, 616–618.

#### Scheme 1



We have explored dioxygen binding to manganese(II) complexes with the hybrid tripodal ligands H<sub>5</sub>bupa and H<sub>3</sub>bpaa (Schemes 1 and 2). Both ligands utilize the carboxamidopyridyl moieties introduced by Masuda et al. and at least one other anionic donor from either a

Scheme 2. Synthetic Route to the Hybrid Ligand H<sub>3</sub>bpaa<sup>a</sup>

<sup>a</sup> Conditions: (a) C<sub>7</sub>H<sub>9</sub>N, Et<sub>3</sub>N, THF, 67 °C, 76%; (b) C<sub>6</sub>H<sub>10</sub>, 20% Pd(OH)<sub>2</sub>/C, EtOH, 78 °C, 69%; (c) C<sub>8</sub>H<sub>7</sub>BrFNO, Et<sub>3</sub>N, THF, 67 °C, 92%.

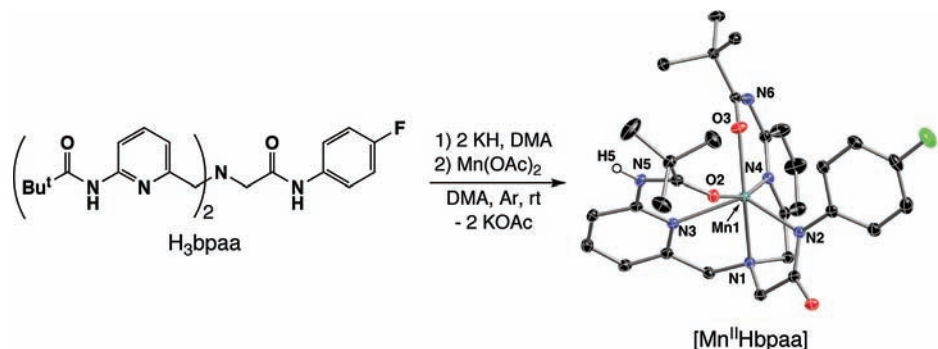


**Figure 11.** Synthetic details and molecular structure for [Mn<sup>II</sup>Hbpaa]. Selected distances (Å): Mn1–N1, 2.287(1), Mn1–N2, 2.157(1), Mn1–N3, 2.279(1), Mn1–N4, 2.266(2), Mn1–O2, 2.247(1), Mn1–O3, 2.047(1).

deprotonated amide or urea. This design takes advantage of an anionic primary coordination sphere, which should aid in the binding of dioxygen, and H-bonding networks within the secondary coordination sphere to stabilize M–O<sub>2</sub> adducts directly from dioxygen. We have shown that [Mn<sup>II</sup>H<sub>2</sub>bupa]<sup>–</sup> reacts with dioxygen to form a peroxo adduct (Scheme 1), which further reacts with aldehydes to afford ketones.<sup>36</sup> These results were the first to show that monomeric manganese–peroxo complexes can synthetically be prepared from a manganese(II) complex and dioxygen at room temperature.

More recently, we have explored similar processes with the neutral complex [Mn<sup>II</sup>Hbpaa], which uses a new ligand [Hbpaa]<sup>2–</sup>, whose synthesis is outlined in Scheme 2. The solid-state structure of [Mn<sup>II</sup>Hbpaa] determined by XRD (Figure 11) reveals a six-coordinate complex in a distorted octahedral geometry. Four of the coordination sites are occupied by N donors from the [Hbpaa]<sup>2–</sup> ligand. The remaining two positions are occupied with the O atoms from the appended carboxamido groups, which adopt conformations such that their carbonyl moieties are positioned toward the metal center. The O atoms bind to the manganese(II) center in different ways, a result of the protonation states of the carboxamide groups. One is deprotonated, resulting in the Mn1–O3 bond distance of 2.047(1) Å, whereas a significantly longer Mn1–O2 bond of 2.247(1) Å is observed for a protonated carboxamide group.

Treating [Mn<sup>II</sup>Hbpaa] with excess O<sub>2</sub> at room temperature showed no evidence of oxidation, which we ascribed to the manganese center being coordinatively saturated.<sup>37</sup> However, when the same reaction was repeated in the presence of 1,2-diphenylhydrazine (DPH), a known

H-atom source,<sup>38</sup> a new species was observed, which we propose is a manganese(III)–peroxo intermediate ([Mn<sup>III</sup>H<sub>2</sub>bpaa(O<sub>2</sub>)]). Spectroscopic measurements support this assignment: after the addition of dioxygen to [Mn<sup>II</sup>Hbpaa], a new parallel-mode electron paramagnetic resonance (EPR) signal appeared at a *g* value of 8.15 with a six-line hyperfine splitting pattern with *a* = 57.7 G (Figure 12A). Variable-temperature studies indicated that this signal arises from a ground-state doublet with a *D* value of –2.0(3) cm<sup>–1</sup> and an *E/D* of 0.13. In addition, the absorbance spectrum measured at room temperature (Figure 12B) has bands at λ<sub>max</sub> = 590 nm (58 M<sup>–1</sup> cm<sup>–1</sup>) and 460 nm (sh):<sup>39</sup> taken together these spectroscopic results are nearly the same as those observed for [Mn<sup>III</sup>H<sub>3</sub>bupa(O<sub>2</sub>)]<sup>–</sup> and are consistent with a monomeric manganese(III)–peroxo complex. Isotopic labeling experiments also support the formulation of this species as [Mn<sup>III</sup>H<sub>2</sub>bpaa(O<sub>2</sub>)]. The generation of [Mn<sup>III</sup>–H<sub>2</sub>bpaa(O<sub>2</sub>)] with <sup>16</sup>O<sub>2</sub> produces a new peak in the FTIR spectrum at 891 cm<sup>–1</sup> and a strong ion with a mass-to-charge ratio of 633.2 (633.2) in the electrospray ionization mass spectrum (ESI-MS): these features shift to 839 cm<sup>–1</sup> and 637.1 (637.2) when samples are prepared with <sup>18</sup>O<sub>2</sub>.

[Mn<sup>III</sup>H<sub>2</sub>bpaa(O<sub>2</sub>)] has reactivity similar to those reported for other metal–peroxo complexes. For instance, treating [Mn<sup>III</sup>H<sub>2</sub>bpaa(O<sub>2</sub>)] with cyclohexanecarboxaldehyde afforded cyclohexanone in 67% yield. We have also found that cyclohexanone is formed when [Mn<sup>II</sup>Hbpaa] and the substrate are exposed to excess O<sub>2</sub> at room temperature. Presumably, formation of the manganese(III)–peroxo complex precedes product formation, yet at present, we have not been able to detect [Mn<sup>III</sup>H<sub>2</sub>bpaa(O<sub>2</sub>)] under these reaction conditions.

(36) Shook, R. L.; Gunderson, W. A.; Greaves, J.; Ziller, J. W.; Hendrich, M. P.; Borovik, A. S. *J. Am. Chem. Soc.* **2008**, *130*, 8888–8889.

(37) [Mn<sup>II</sup>Hbpaa] also reacts directly with H<sub>2</sub>O<sub>2</sub> at room temperature in DMSO to produce [Mn<sup>III</sup>H<sub>2</sub>bpaa(O<sub>2</sub>)] in nearly quantitative yields.

(38) [Mn<sup>III</sup>H<sub>2</sub>bpaa(O<sub>2</sub>)] was also produced with indene and fluorine as the H-atom sources, whereas no reactions were observed in the presence of DHA and xanthene.

(39) The absorbance spectrum for [Mn<sup>III</sup>H<sub>2</sub>bpaa(O<sub>2</sub>)] was prepared by treating [Mn<sup>II</sup>Hbpaa] with H<sub>2</sub>O<sub>2</sub> at room temperature. Spectra obtained with dioxygen were similar but contained a strong absorbance from azobenzene.

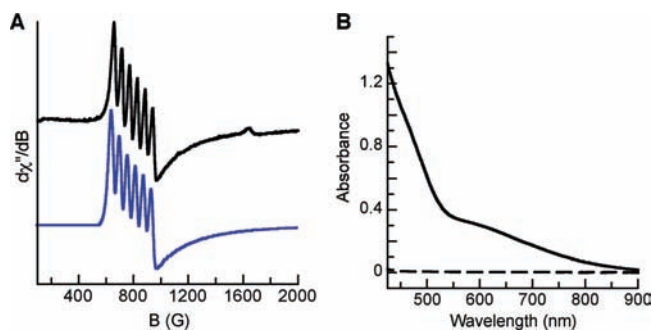


**Figure 12.** Parallel-mode EPR spectrum (black) and simulation (blue) of  $[\text{Mn}^{\text{III}}\text{H}_2\text{bpaa}(\text{O}_2)]$  (2 mM in THF) recorded at 2.2 K (A) and absorbance spectra of  $[\text{Mn}^{\text{II}}\text{H}_2\text{bpaa}]$  (---) and  $[\text{Mn}^{\text{III}}\text{H}_2\text{bpaa}(\text{O}_2)]$  (—) (10 mM in DMSO) measured at room temperature (B). EPR parameters: microwave frequency and power, 9.26 GHz, 0.2 mW; modulation, 10 G. EPR simulation parameters:  $S = 2$ ,  $g = 2.0$ ,  $D = -2 \text{ cm}^{-1}$ ,  $E/D = 0.13$ ,  $A = 160 \text{ MHz}$ .

### Dioxygen Activation: Generation of Metal–Oxo Intermediates

The previous sections described approaches to stabilize dioxygen adducts to metal complexes. Closely related to these efforts are investigations into the fate of the  $\text{M}-\text{O}_2$  adduct, in particular what is produced after breakage of the  $\text{O}-\text{O}$  bond. This is an especially important question because of the pivotal role oxidation that has in industrial and biological processes. The consensus view is that  $\text{O}-\text{O}$  bond cleavage produces high-valent metal species, many of which have terminal oxo ligands that directly oxidize substrates. One mechanism often invoked is that for the cytochrome P450 compounds, whereby reduction of dioxygen to a terminal oxo–iron species (compound 1) proceeds through several intermediates via the controlled flow of electrons and protons into the active site. The secondary coordination sphere is instrumental in the activation process, with site isolation and H-bonding networks being needed to achieve the selective oxidation of substrates. For instance, substrate binding in P450, which initiates the catalytic cycles, often utilizes H bonds formed between the substrate and amino acids within the active site. H bonds involving the hydroxy group of a nearby threonine (Thr-252) stabilize the  $\text{Fe}-\text{O}_2$  moiety (Figure 13A).<sup>40,41</sup> This H bond also appears to assist in  $\text{O}-\text{O}$  bond cleavage because Thr-252 is essential for the reduction of dioxygen to peroxide during the initial stages of dioxygen activation. Moreover, a H-bonding network, created with amino acid residues and structural water molecules near the iron center, provides a pathway for protons to traverse through the active site during turnover.

A similar role has been proposed for H bonds in the active sites of peroxidases and catalases, where H-bonding to  $\text{Fe}-\text{O}_2$  is believed to polarize the peroxy group, helping facilitate heterolytic  $\text{O}-\text{O}$  bond cleavage.<sup>42</sup> Moreover, H bonds are formed to the high-valent  $\text{Fe}^{\text{IV}}=\text{O}$  units that are

generated in the catalytic mechanism of iron–heme peroxidase.<sup>43,44</sup> A variety of spectroscopic and low-temperature structural studies on compounds I and II of horseradish peroxidases (HRPs) have indicated that the oxo of the ferryl group is H-bonded to amino acid residues in the active site (Figure 13B).<sup>45</sup> This has led to the proposal that peroxidase activity is partially regulated by this H-bonding interaction.

### Secondary Coordination Sphere, Synthetic Systems, and Dioxygen Activation

Inspired by the findings from metalloproteins, we sought to develop synthetic systems whereby the activation of dioxygen is controlled, at least in part, by H-bonding networks in the secondary coordination sphere.<sup>46</sup> Our objectives were to understand how the H bonds affected the metal-mediated activation process and the subsequent dioxygen-derived species produced. To accomplish these goals, we designed a series of tripodal ligands that when bonded to transition-metal ions, created rigid H-bonding cavities around vacant coordination sites. The rationale behind our ligands has been reported<sup>46d,e</sup> and will only briefly be discussed. The key component in our designs is the urea moieties, which was a logical choice based on the vast literature showing their strong tendency to H-bond in both solution and the solid state. In most other systems, the two NH moieties are actively involved in H-bonding to other functional groups. Our systems use the urea units in a different way because of the need to simultaneously bind a metal ion and create an intramolecular H-bonding network. The design principles are illustrated using the parent symmetrical tripodal compound, tris[*N'*-*tert*-butylureayl-*N*-ethylethylamine] ( $\text{H}_6\text{buea}$ ; Figure 14), in which the  $\alpha\text{NH}$  groups are deprotonated to form a highly anionic metal-ion-binding pocket and the remaining parts of the urea groups form the scaffolding of a cavity. Be aware that the preferred conformation of the urea groups place the  $\alpha'\text{NH}$  groups within the interior of the cavity, positioning them proximal to the metal center and in the proper location to H-bond with external ligands. In addition, using bulky R groups off the  $\alpha'$ -N atoms isolates the metal centers and limits unwanted metal–metal interactions.

Our first efforts led to the preparation of monomeric iron(III) and manganese(III) complexes with terminal oxo ligands. These types of complexes had been problematic to isolate because of the strong thermodynamic tendency of

(43) Mukai, M.; Nagano, S.; Tanaka, M.; Ishimori, K.; Morishima, I.; Ogura, T.; Watanabe, Y.; Kitagawa, T. *J. Am. Chem. Soc.* **1997**, *119*, 1758–1766 and references cited therein.

(44) (a) Fülöp, V.; Phizackerley, R. P.; Soltis, S. M.; Clifton, I. J.; Wakatsumi, S.; Erman, J.; Hajdu, J.; Edwards, S. L. *Structure* **1994**, *2*, 201–208. (b) Bonagura, C. A.; Bhaskar, B.; Shimizu, H.; Li, H.; Sundaramoorthy, M.; McRee, D. E.; Goodin, D. B.; Poulos, T. L. *Biochemistry* **2003**, *42*, 5600–5608.

(45) Berglund, G. I.; Carlsson, G. H.; Smith, A. T.; Szöke, H.; Henriksen, A.; Hajdu, J. *Nature* **2002**, *417*, 463–466.

(46) Selected references: (a) Hammes, B. S.; Young, V. G.; Borovik, A. S. *Angew. Chem., Int. Ed.* **1999**, *38*, 666–669. (b) MacBeth, C. E.; Golombek, A. P.; Young, V. G., Jr.; Yang, C.; Kuczera, K.; Hendrich, M. P.; Borovik, A. S. *O2 Science* **2000**, *289*, 938–941. (c) Gupta, R.; Borovik, A. S. *J. Am. Chem. Soc.* **2003**, *125*, 13234–13242. (d) MacBeth, C. E.; Gupta, R.; Mitchell-Koch, K. R.; Young, V. G.; Lushington, G. H.; Thompson, W. H.; Hendrich, M. P.; Borovik, A. S. *J. Am. Chem. Soc.* **2004**, *126*, 2556–2567. (e) Borovik, A. S. *Acc. Chem. Res.* **2005**, *38*, 54–61. (f) Shook, R. L.; Borovik, A. S. *Chem. Commun.* **2008**, 6095–6107.

(40) (a) Martinis, S. A.; Atkins, W. M.; Stayton, P. S.; Sligar, S. G. *J. Am. Chem. Soc.* **1989**, *111*, 9252–9253. (b) Gerber, N. C.; Sligar, S. G. *J. Am. Chem. Soc.* **1992**, *114*, 8742–8743. (c) Sono, M.; Roach, M. P.; Coulter, E. D.; Dawson, J. H. *Chem. Rev.* **1996**, *96*, 2841–2887.

(41) (a) Schlichting, I.; Berendzen, J.; Chu, K.; Stock, A. M.; Maves, S. A.; Benson, D. E.; Sweet, R. M.; Ringe, D.; Pestko, G. A.; Sligar, S. G. *Science* **2000**, *287*, 1615–1622. (b) Nagano, S.; Poulos, T. L. *J. Biol. Chem.* **2005**, *280*, 31659–31663.

(42) Poulos, T. L. *Adv. Inorg. Biochem.* **1988**, *7*, 1–36.



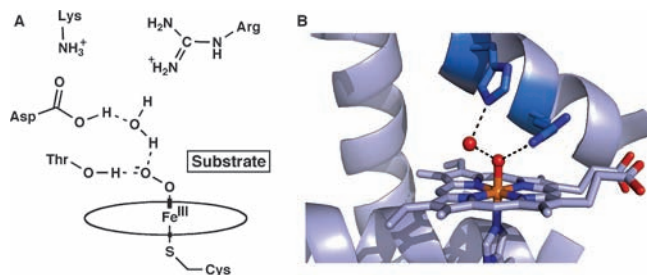


**Figure 13.** Active sites of cytochrome P450 (A) and compound 1 of horseradish peroxidase (PDB, 1HCH) highlighting the intramolecular hydrogen-bonding networks surrounding the iron centers.

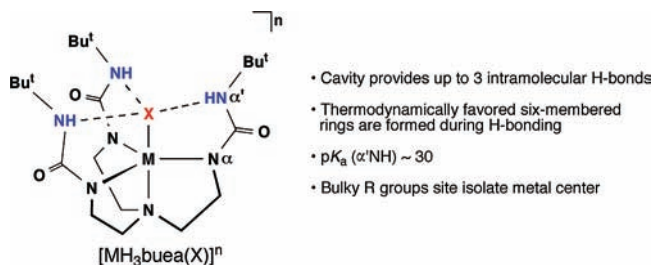


**Figure 14.** Design criteria for complexes with the H-bonding ligand  $[H_3buea]^{3-}$ .

these metal ions to form  $M-\mu-O-M$  species. Moreover, there are longstanding theoretical predictions that metal centers with four or more  $d$  electrons would not be able to form terminal oxo species, especially if they were high-spin complexes (vide infra). Despite these concerns, we were successful in stabilizing and isolating  $[M^{III}H_3buea(O)]^{2-}$  directly from the activation of dioxygen (Scheme 3). Isotopic labeling studies confirmed that dioxygen was the source of the oxo ligand; a  $\nu(Fe-O)$  peak at  $671\text{ cm}^{-1}$  was observed for  $[Fe^{III}H_3buea(^{16}O)]^{2-}$ , which shifted to  $645\text{ cm}^{-1}$  in  $[Fe^{III}H_3buea(^{18}O)]^{2-}$ . Similarly,  $[Mn^{III}H_3buea(^{16}O)]^{2-}$  had a  $\nu(Mn-O)$  of  $700\text{ cm}^{-1}$ , which moved to  $672\text{ cm}^{-1}$  in the  $^{18}O$  isotopomer.

The molecular structures for the two  $[M^{III}H_3buea(O)]^{2-}$  were determined in the solid state by XRD methods to reveal trigonal-bipyramidal geometries around the metal centers (Figure 15). The oxo ligand binds in an axial position and resides within the H-bonding cavity formed by the  $[H_3buea]^{3-}$  ligand. Distances between heavy atoms are often used to gauge whether H bonds are present in the solid state. Using this criterion, there is strong metrical evidence for intramolecular H bonds, with each complex having  $O1 \cdots \alpha'N$  distances of less than  $2.9\text{ \AA}$ . Further support came from solid-state Fourier transform infrared (FTIR) studies that showed a shift to lower energy and broadening of the  $\nu(N-H)$  peaks compared to  $H_3buea$ , features that are indicative of strong H bonds. Notice that the three urea arms of  $[H_3buea]^{3-}$  are symmetrically distributed around the  $M^{III}-O$  units in the solid state, which we proposed also occurs in solution. This premise is supported by the axial EPR spectrum obtained for  $[Fe^{III}H_3buea(O)]^{2-}$  ( $g_{x,y} = 6.0$ ,  $g_z = 2.0$ ;  $E/D = 0$ ), data that are consistent with a complex having  $C_3$  symmetry. Additional magnetic measurements on both complexes indicated that  $[Fe^{III}H_3buea(O)]^{2-}$  and  $[Mn^{III}H_3buea(O)]^{2-}$  have spin ground states of  $S = 5/2$  and  $S = 2$ , respectively.

At first glance, the high-spin character of these complexes was surprising because most known complexes with terminal

oxo ligands are low-spin, a finding that agrees with most bonding schemes. All theories have stipulated that multiple bonds are needed between the oxo ligand and a metal center to prepare stable monomeric oxo-metal complexes.<sup>47</sup>  $\pi$  bonds arise between filled  $p$  orbitals on the oxo ligand and vacant  $d$  orbitals on the metal ion. Calculations predict that low-spin oxo-metal complexes having  $C_4v$  symmetry are isolable for metal ions with less than three  $d$  electrons because the initial electrons are housed in a nonbonding orbital (Figure 16A).<sup>48</sup> More electron-rich systems populate anti-bonding  $\pi$  orbitals, leading to reactive species. Mayer and Thorn showed that  $C_3$ -symmetric oxo-metal complexes with up to four  $d$  electrons are also accessible, again provided that the complexes are low-spin (Figure 16B).<sup>48,49</sup>

The properties associated with  $[Fe^{III}H_3buea(O)]^{2-}$  and  $[Mn^{III}H_3buea(O)]^{2-}$  clearly do not follow the general principles used to describe other oxo-metal complexes. We have probed our systems to understand the fundamental properties associated with the  $M-O$  unit. A combination of spectroscopic and theoretical studies supports the concept that the intramolecular H-bonding network within the complexes has a significant effect on the overall stability of the complexes. Theory showed that the intramolecular H bonds in a truncated version of  $[Fe^{III}H_3buea(O)]^{2-}$  contributed  $25\text{ kcal/mol}$  to the stability of the complex.<sup>50</sup> This stabilization was somewhat offset by a decrease in the  $Fe-O$  bond energy by  $19\text{ kcal/mol}$  compared to that found in a computer-generated control system that does not contain intramolecular H bonds (Figure 17). The weakening of the  $Fe-O$  interaction  $[Fe^{III}H_3buea(O)]^{2-}$  was credited exclusively to a reduction in  $\pi$  bonds between the iron center and oxo ligand to the extent that there was essentially no multiple-bond character present. Thus, these findings show that in some cases H bonds can replace  $\pi$  bonds to oxo-metal complexes, a result that can have profound implications on the development of new oxidation catalysts and understanding of functions of metalloproteins. We have argued that it may be possible to tune the properties and reactivity of oxo-metal species via modulation in the H-bonding networks within the secondary coordination sphere.<sup>46d-f</sup> For example, adjustments in the metal-oxo bond energy, as seen in  $[Fe^{III}H_3buea(O)]^{2-}$ , could lead to new means of controlling the reactivity and selectivity of oxidation reagents. Moreover, it may be possible to develop structure-function correlations based on the type of H-bonding networks surrounding a metal-oxo unit.

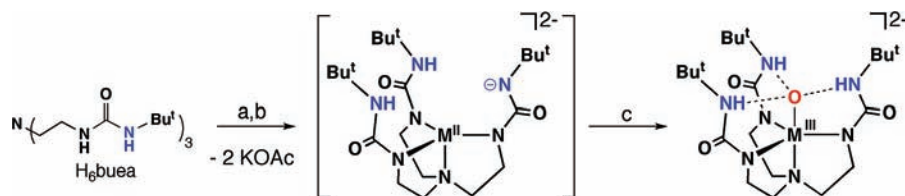
(47) (a) Nugent, W. A.; Mayer, J. M. *Metal-Ligand Multiple Bonds: The Chemistry of Transition Metal Complexes Containing Oxo, Nitrido, Imido, Alkylidene, or Alkylidyne Ligands*, 1st ed.; Wiley: New York, 1988. (b) Griffith, W. P. *Coord. Chem. Rev.* **1970**, *5*, 459–517. (c) Gulliver, D. J.; Levason, W. *Chem. Soc. Rev.* **1982**, *46*, 1–127.

(48) Mayer, J. M.; Thorn, D. L.; Tulip, T. H. *J. Am. Chem. Soc.* **1985**, *107*, 7454–7462 and references cited therein.

(49) Selected examples of other oxo complexes with at least four  $d$  electrons:<sup>48</sup>(a) Wilkinson, G.; Hay-Motherwell, R.; Hussian-Bates, B.; Hursthouse, M. B. *Polyhedron* **1993**, *12*, 2009–2012. (b) Cheng, W.-C.; Yu, W.-Y.; Cheung, K.-K.; Che, C.-M. *J. Chem. Soc., Dalton Trans.* **1994**, 57–62. (c) Welch, T. W.; Ciftan, S. A.; White, P. S.; Thorp, H. H. *Inorg. Chem.* **1997**, *36*, 4812–4821. (d) Spaltenstein, E.; Conry, R. R.; Critchlow, S. C.; Mayer, J. M. *J. Am. Chem. Soc.* **1989**, *111*, 8741–8742. (e) Rohde, J.-U.; In, J.-H.; Lim, M. H.; Brennessel, W. W.; Bukowski, M. R.; Stubna, A.; Münck, E.; Wam, W.; Que, L., Jr. *Science* **2003**, *299*, 1037–1039. (f) England, J.; Martinho, M.; Farquhar, E. R.; Frisch, J. R.; Bominaar, E. L.; Munck, E.; Que, L., Jr. *Angew. Chem., Int. Ed.* **2009**, *48*, 3622–3626.

(50) Dey, A.; Hocking, R. K.; Larsen, P. L.; Borovik, A. S.; Hedman, B.; Hodgson, K. O.; Solomon, E. I. *J. Am. Chem. Soc.* **2006**, *128*, 9825–9833.

**Scheme 3.** Synthetic Procedure for the Isolation of  $[\text{M}^{\text{III}}\text{H}_3\text{buea}(\text{O})]^{2-}$  ( $\text{M}^{\text{III}} = \text{Fe}, \text{Mn}$ )<sup>a</sup>



<sup>a</sup> Conditions: (a) 4KH, DMA, Ar, rt; (b)  $\text{M}(\text{OAc})_2$ , DMA, Ar, rt; (c)  $1/2\text{O}_2$ , DMA, rt.

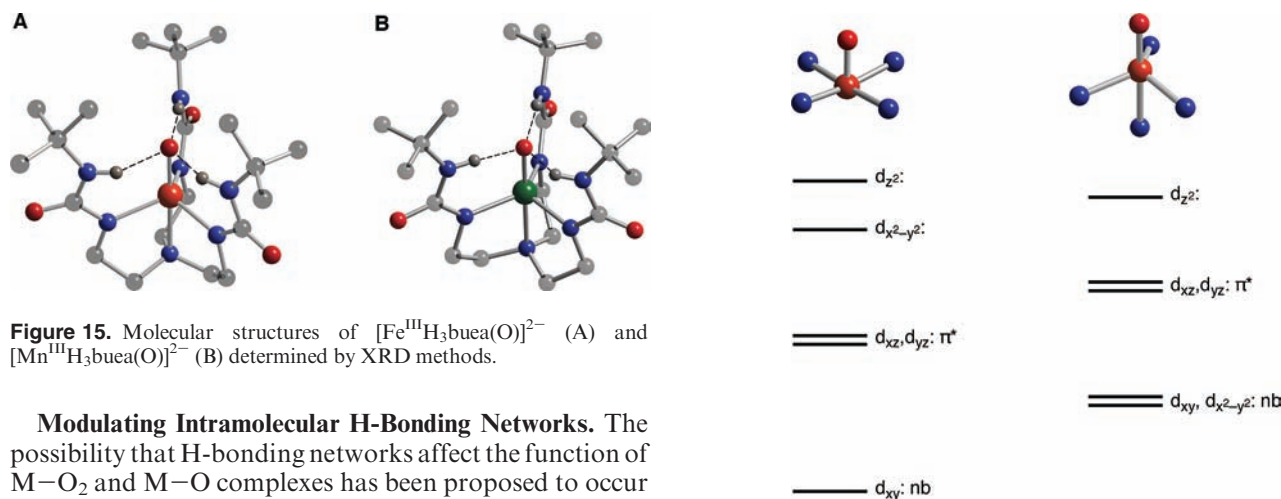


**Figure 15.** Molecular structures of  $[\text{Fe}^{\text{III}}\text{H}_3\text{buea}(\text{O})]^{2-}$  (A) and  $[\text{Mn}^{\text{III}}\text{H}_3\text{buea}(\text{O})]^{2-}$  (B) determined by XRD methods.

**Modulating Intramolecular H-Bonding Networks.** The possibility that H-bonding networks affect the function of  $\text{M}-\text{O}_2$  and  $\text{M}-\text{O}$  complexes has been proposed to occur in metalloproteins, where active-site structures and protein function are known.<sup>51</sup> A series of heme proteins nicely illustrate this possibility. Myoglobin, heme oxygenase, and horseradish peroxidase (HRP) all have the same square-pyramidal geometries within their primary coordination spheres and form  $\text{M}-\text{O}_2$  adducts. However, myoglobin reversibly binds dioxygen, HRP cleaves the  $\text{O}-\text{O}$  bond to destroy peroxide, and heme oxygenase also breaks the  $\text{O}-\text{O}$  bond but to oxidize the porphyrin ring during heme catabolism. These differences in function could be related to the varied H-bonding networks surrounding the iron centers within their respective active sites.

We have developed systems to examine the effects of varied H-bonding networks on dioxygen activation in synthetic complexes.<sup>52</sup> A straightforward design concept was employed for the metal-containing precursors: a series of four cobalt(II) complexes were prepared with trigonal-monopyramidal coordination geometries but tunable H-bonding networks within their secondary coordination spheres. The investigation required four ligands, each with a trianionic metal-binding pocket

**Figure 16.** Qualitative orbital diagrams for metal-oxo complexes with  $\text{C}_{4v}$  (left) and  $\text{C}_3$  symmetry (right) (adapted from Mayer and Thorn).<sup>48</sup>

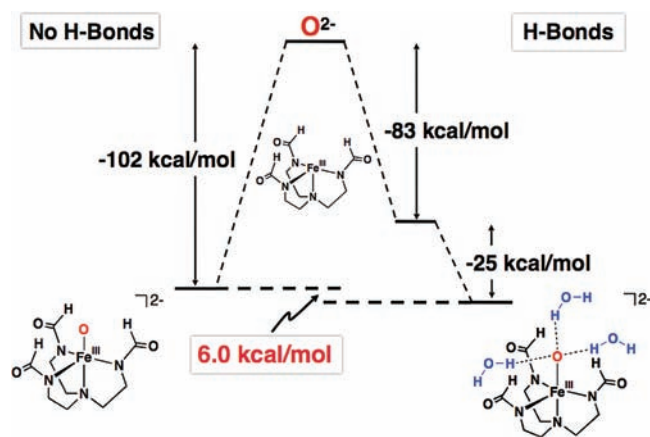


**Figure 17.** Bonding decomposition scheme for the  $\text{Fe}^{\text{III}}-\text{O}$  complex illustrating the effects of the intramolecular H-bonding network.

but differing in the number of H-bond donors. Building on the work that we had done on the symmetrical urea-based ligand  $[\text{H}_3\text{buea}]^{3-}$  and its amidate counterpart  $[\text{O}]^{3-}$ , we prepared the two hybrid ligands  $[\text{H}_2\text{I}]^{3-}$  and  $[\text{H}1]^{3-}$  (Figure 18). Their corresponding cobalt(II) complexes were synthesized and characterized to show similar molecular and electronic structures. Yet, differences in the reactivity with dioxygen were observed throughout the series of complexes.

Treating  $[\text{Co}^{\text{II}}\text{H}_3\text{buea}]^-$  and  $[\text{Co}^{\text{II}}\text{H}_2\text{I}]^-$  with dioxygen (0.5 equiv) under the same experimental conditions (Figure 18) gave the  $\text{Co}^{\text{III}}-\text{OH}$  complexes in yields of greater than 70%. Isotopic labeling studies and spectroscopic measurements confirmed the identity of these

(51) Selected examples: (a) Holmes, M. A.; Stenkamp, R. E. *J. Mol. Biol.* **1991**, *220*, 723–737. (b) Fülöp, V.; Phizackerley, R. P.; Soltis, S. M.; Clifton, I. J.; Wakatsuki, S.; Erman, J.; Hajdu, J.; Edwards, S. L. *Structure* **1994**, *2*, 201–208. (c) Mukai, M.; Nagano, S.; Tanaka, M.; Ishimori, K.; Morishima, I.; Ogura, T.; Watanabe, Y.; Kitagawa, T. *J. Am. Chem. Soc.* **1997**, *119*, 1758–1766 and references cited therein. (d) Dunitz, B. D.; Beachy, M. D.; Cao, Y.; Whittington, D. A.; Lippard, S. J.; Friesner, R. A. *J. Am. Chem. Soc.* **2000**, *122*, 2828–2839. (e) Gherman, B. F.; Dunitz, B. D.; Whittington, D. A.; Lippard, S. J.; Friesner, R. A. *J. Am. Chem. Soc.* **2001**, *123*, 3836–3837. (f) Du Bois, J.; Mizoguchi, T. J.; Lippard, S. J. *Coord. Chem. Rev.* **2000**, *200–202*, 443–485. (g) Berglund, G. I.; Carlsson, G. H.; Smith, A. T.; Szöke, H.; Henriksen, A.; Hajdu, J. *Nature* **2002**, *417*, 463–468. (h) Tomchick, D. R.; Phan, P.; Cymborowski, M.; Minor, W.; Holman, T. R. *Biochemistry* **2001**, *40*, 7509–7517.

(52) Lucas, R. L.; Mukherjee, J.; Zart, M. K.; Sorrell, T. N.; Powell, D. R.; Borovik, A. S. *J. Am. Chem. Soc.* **2006**, *128*, 15476–15489.

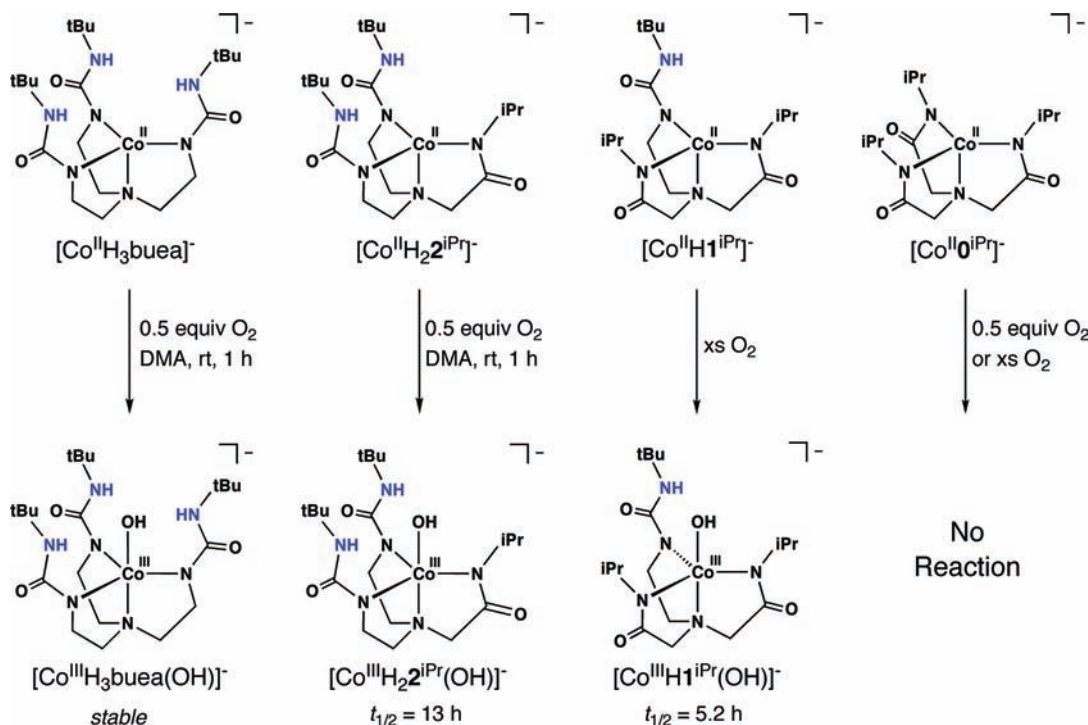


**Figure 18.** Summary of the dioxygen reactivity for a series of cobalt(II) complexes with varied H-bonding networks.

complexes.  $[Co^{II}H1]^-$ , a complex containing only one H-bond donor, showed no appreciable reactivity with dioxygen under these conditions. Excess dioxygen was needed to initiate a reaction, with the first observable species proposed to be a cobalt(II)–superoxo species with an  $S = 1/2$  spin ground state. This complex converted to an intermediate that had spectroscopic properties consistent with a  $Co^{III}-OH$  complex, but it was too unstable to isolate in pure form. The final complex in the series,  $[Co^{II}0]^-$  contained no H-bond donors and did not react with dioxygen under any conditions. Note that we have ruled out steric constraints of the cavity as the reason for this lack of dioxygen reactivity. We have numerous examples of complexes with  $[0]^{3-}$  being able to form five-coordinate complexes, including  $[Co^{II}0(CN)_2]^{2-}$ , which was isolated and structurally characterized.

The trigonal-monopyramidal cobalt(II) complexes have different levels of reactivity toward dioxygen despite their nearly identical primary coordination spheres. We have suggested that this difference is caused in large part by the intramolecular H-bonding networks within the secondary coordination sphere that assist in the binding of  $O_2$ , leading to activation of  $O_2$  and formation of the  $Co^{III}-OH$  complexes. The data showed a distinct correlation between the number of H bonds and  $O_2$  binding/activation. The connection is apparent when the reactivities of  $[Co^{II}H_22iPr]^-$  and  $[Co^{II}H1iPr]^-$  are compared, both of which are capable of forming intramolecular H bonds.  $[Co^{II}H_22iPr]^-$ , with two H-bond donors, reacts at lower  $O_2$  concentrations compared with  $[Co^{II}H1iPr]^-$ , which only has the possibility of forming one intramolecular H bond. An additional H-bond donor in  $[Co^{II}H_22iPr]^-$  would assist in dioxygen binding, the essential first step in metal-mediated  $O_2$  activation. Moreover,  $[Co^{II}0]^-$  does not bind dioxygen and is the only complex in the series that is incapable of forming intramolecular H bonds. Finally,

there is a clear relationship between the stability of the  $Co^{III}-OH$  complexes and the number of intramolecular H-bond donors.  $[Co^{III}H_3buea(OH)]^-$ , with three H-bond donors, was by far the most stable complex in solution, leading to its crystallization. The other complexes reacted to such an extent in solution that crystallization was not possible. Two reasons could account for the observed stabilities: (1) increasing the number of H bonds to the  $Co^{III}-OH$  unit would lower its nucleophilicity, rendering it less reactive; (2) the additional H bonds with an intramolecular network would rigidify the cavity structure, limiting further reactivity with external species.

The structure–function relationships observed in our cobalt(II) complexes support the idea that the activity of a metalloprotein is linked to the H-bonding networks within secondary coordination spheres. This relationship is especially pertinent in systems involving  $O_2$  binding and activation. It appears likely that other correlations will be established as more data emerge from both biological and synthetic systems. For example, there are now specific examples of engineered metalloproteins, in which changes in H-bonding networks within active sites affect the physical properties and reactivity.<sup>53</sup> Moreover, other synthetic systems have been reported that show strong links between H bonds and physical properties, such as redox potentials and  $pK_a$  values.<sup>31,35</sup>

**Relationship between the Basicity of the Oxo Ligand and Chemical Reactivity.** The isolation of  $[M^{III}H_3buea(O)]^{2-}$  has led to the formation of related complexes, namely, the monomeric  $M^{III/II}-OH$  complexes  $[M^{III}H_3buea(OH)]^-$  and  $[M^{II}H_3buea(OH)]^{2-}$ , which are stable and have been completely characterized, including their molecular

(53) (a) Miller, A. F. *Acc. Chem. Res.* **2008**, *41*, 501–510. (b) Jackson, T. A.; Brunold, T. C. *Acc. Chem. Res.* **2004**, *37*, 461–470.

structures by XRD. Both iron and manganese hydroxo complexes have trigonal-bipyramidal coordination geometries comparable to those of the parent metal–oxo complexes with intramolecular H-bonding networks surrounding the M–OH units. We have also been able to detect  $[\text{Mn}^{\text{IV}}\text{H}_3\text{buea}(\text{O})]^-$ , a rare example of a manganese(IV)–oxo complex. Similar to the  $\text{M}^{\text{III}}\text{–O}$  complexes, the  $\text{M}^{\text{III/II}}\text{–OH}$  and  $\text{Mn}^{\text{IV}}\text{=O}$  complexes are all high-spin. A more complete description of the preparative details and properties of these complexes has been reviewed recently.<sup>46c,f</sup>

We have used these complexes to investigate C–H cleavage by metal–oxo complexes.<sup>46c,54</sup> This type of reaction has a wide variety of chemical and biology applications but is one of the most difficult chemical transformations, mostly because of the high dissociation energies of C–H bonds.<sup>55</sup> In many substrates, the homolytic bond dissociation energies are greater than 90 kcal/mol, making them thermodynamically difficult to cleave. Like many researchers, we have turned to biology to gain insights into how to accomplish this transformation. Numerous metalloproteins have evolved that achieve this reaction, and most studies suggest that metal–oxo species, derived from the activation of dioxygen, are the active species involved in C–H bond cleavage. The oxidation strength of metal–oxo complexes is usually expressed in terms of redox potentials, with compounds having higher redox potentials being stronger oxidants. Our metal–oxo complexes are also derived from dioxygen and are able to cleave C–H bonds; however, their redox potentials are unusually low for complexes that oxidize substrates. For example, the  $[\text{Mn}^{\text{IV/III}}\text{H}_3\text{buea}(\text{O})]^{-/2-}$  and  $[\text{Mn}^{\text{V/IV}}\text{H}_3\text{buea}(\text{O})]^-$  redox couples are at  $-1.0$  and  $-0.076$  V vs  $\text{Cp}_2\text{Fe}^+/\text{Cp}_2\text{Fe}$ . Moreover, we were unable to observe the  $[\text{Mn}^{\text{III/II}}\text{H}_3\text{buea}(\text{O})]^{2-/3-}$  process, suggesting that it is lower than  $-2.0$  V vs  $\text{Cp}_2\text{Fe}^+/\text{Cp}_2\text{Fe}$ . However,  $[\text{Mn}^{\text{III}}\text{H}_3\text{buea}(\text{O})]^{2-}$  reacts with substrates containing a C–H bond of  $\sim 80$  kcal/mol, and  $[\text{Mn}^{\text{IV}}\text{H}_3\text{buea}(\text{O})]^-$  cleaves C–H bonds of  $\sim 90$  kcal/mol.

The findings with manganese–oxo complexes suggested that redox potentials alone were not sufficient to fully explain the observed reactivity. To gain a more detailed understanding of our systems, we adapted the approach pioneered by Mayer to use thermodynamic cycles to evaluate the ability of metal–oxo complexes to homolytically cleave C–H bonds.<sup>56</sup> The basis of this approach is to experimentally evaluate the homolytic O–H bond dissociation energies ( $\text{BDE}_{\text{OH}}$ ) of M–OH complexes that are produced after C–H bond homolysis: for this transformation to be thermodynamically achievable, the energy required to cleave the C–H bond must be comparable to that produced in forming a O–H bond.  $\text{BDE}_{\text{OH}}$  can be obtained from the appropriate experimentally determined one-electron redox potentials and  $\text{p}K_{\text{a}}$  values (Figure 19), using eq 1. The constant  $C$  is included in the analysis to account for solvation of the H

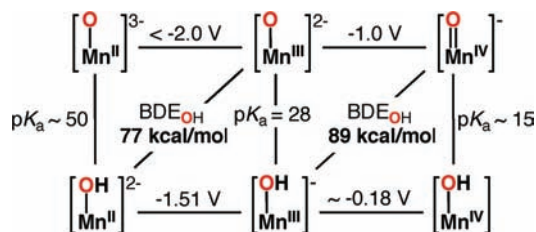


**Figure 19.** Thermodynamic cycles used to evaluate  $\text{BDE}_{\text{OH}}$  for  $[\text{Mn}^{\text{II}}\text{H}_3\text{buea}(\text{OH})]^{2-}$  and  $[\text{Mn}^{\text{III}}\text{H}_3\text{buea}(\text{OH})]^-$ .

atom and is dependent on the solvent and reference used to measure the redox potentials.<sup>57</sup>

$$\text{BDE}_{\text{OH}} = 23.06E_{1/2} + 1.37\text{p}K_{\text{a}} + C \quad (1)$$

The analysis of  $\text{BDE}_{\text{OH}}$  was readily accomplished because the needed Mn–O(H) complexes had already been prepared and characterized as discussed above. From these studies, we found that the oxo ligands in the  $\text{Mn}^{\text{IV/III}}\text{–O}$  complexes were basic, with  $\text{p}K_{\text{a}}$  values of 28.3 and  $\sim 15$  for  $[\text{Mn}^{\text{III}}\text{H}_3\text{buea}(\text{OH})]^-$  and  $[\text{Mn}^{\text{IV}}\text{H}_3\text{buea}(\text{OH})]$ . Taken together with the measured redox potentials, we obtained a  $\text{BDE}_{\text{OH}}$  of 89 kcal/mol for  $[\text{Mn}^{\text{III}}\text{H}_3\text{buea}(\text{OH})]^-$  and 77 kcal/mol for  $[\text{Mn}^{\text{II}}\text{H}_3\text{buea}(\text{OH})]^{2-}$  (Figure 19).<sup>54</sup> It is gratifying to note that these predicted values were in close agreement with what was observed in our reactivity studies between substrates having cleavable C–H bonds and the  $\text{Mn}^{\text{IV/III}}\text{–O}$  complexes.<sup>46c,54</sup>

One of the benefits of these thermodynamic analyses was that they showed the importance that the basicity of the oxo ligand has on C–H bond cleavage. It is clearly evident from our work that the strongly basic character of the oxo groups helped drive the observed reactivity with external substrates. Furthermore, the large difference in basicity for the two manganese–oxo complexes predicted that they should react differently with substrates with differing acidities. The reactivity with 2,4,6-tri-*tert*-butylphenol illustrated this point:  $[\text{Mn}^{\text{IV}}\text{H}_3\text{buea}(\text{O})]^-$  homolytically cleaved the O–H bond, producing the phenoxyl radical and  $[\text{Mn}^{\text{III}}\text{H}_3\text{buea}(\text{OH})]^-$ , whereas the more basic  $[\text{Mn}^{\text{III}}\text{H}_3\text{buea}(\text{O})]^{2-}$  deprotonated the phenol,<sup>58</sup> producing the phenolate anion and  $[\text{Mn}^{\text{III}}\text{H}_3\text{buea}(\text{OH})]^-$ .

The formation of this series of Mn–O(H) complexes also aided in a comparative kinetic analysis of the C–H bond cleavage from 9,10-dihydroanthracene (DHA). For  $[\text{Mn}^{\text{III}}\text{H}_3\text{buea}(\text{O})]^{2-}$  at 20 °C, a corrected second-order rate constant ( $k^{\text{Mn}^{\text{III}}\text{–O}}$ )<sup>12,59</sup> of  $0.48(4) \text{ M}^{-1} \text{ s}^{-1}$  was determined, which is more than 1 order of magnitude larger than the  $k^{\text{Mn}^{\text{IV}}\text{–O}}$  of  $0.026(2) \text{ M}^{-1} \text{ s}^{-1}$  found for  $[\text{Mn}^{\text{IV}}\text{H}_3\text{buea}(\text{O})]^-$ . This result is counter to what would have been predicted based on the  $\text{BDE}_{\text{OH}}$  values for the Mn–OH analogues (Figure 19), in which  $\text{BDE}_{\text{OH}}$  of  $[\text{Mn}^{\text{III}}\text{H}_3\text{buea}(\text{OH})]^-$  is greater than that for  $[\text{Mn}^{\text{II}}\text{H}_3\text{buea}(\text{OH})]^{2-}$  by 12 kcal/mol. Insights into this unexpected finding came from the measured kinetic isotope

(54) Parsell, T. H.; Yang, M.-Y.; Borovik, A. S. *J. Am. Chem. Soc.* **2009**, *131*, 2762–2763.

(55) Stone, K. L.; Borovik, A. S. *Curr. Opin. Chem. Biol.* **2009**, *13*, 114–118.

(56) (a) Mayer, J. M. In *Biomimetic Oxidations Catalyzed by Transition Metal Complexes*; Meunier, B., Ed.; Imperial College Press: London, 2000; pp 1–43. (b) Mayer, J. M. *Annu. Rev. Phys. Chem.* **2004**, *55*, 363–390.

(57) (a) Bordwell, F. G.; Cheng, J.-P.; Ji, G.-Z.; Satish, A. V.; Zhang, X. *J. Am. Chem. Soc.* **1991**, *113*, 9790–9795. (b) Parker, V. D.; Handoo, K. L.; Roness, F.; Tilsted, M. *J. Am. Chem. Soc.* **1991**, *113*, 7493–7498.

(58) 2,4,6-Tri-*tert*-phenol:  $\text{BDE}_{\text{OH}} = 85$  kcal/mol,  $\text{p}K_{\text{a}} = 18$ . Bordwell, F. G.; Zhang, X.-M. *J. Org. Chem.* **1995**, *8*, 529–535.

(59) The second-order rate constants were normalized for the four reactive C–H bonds per substrate molecule.

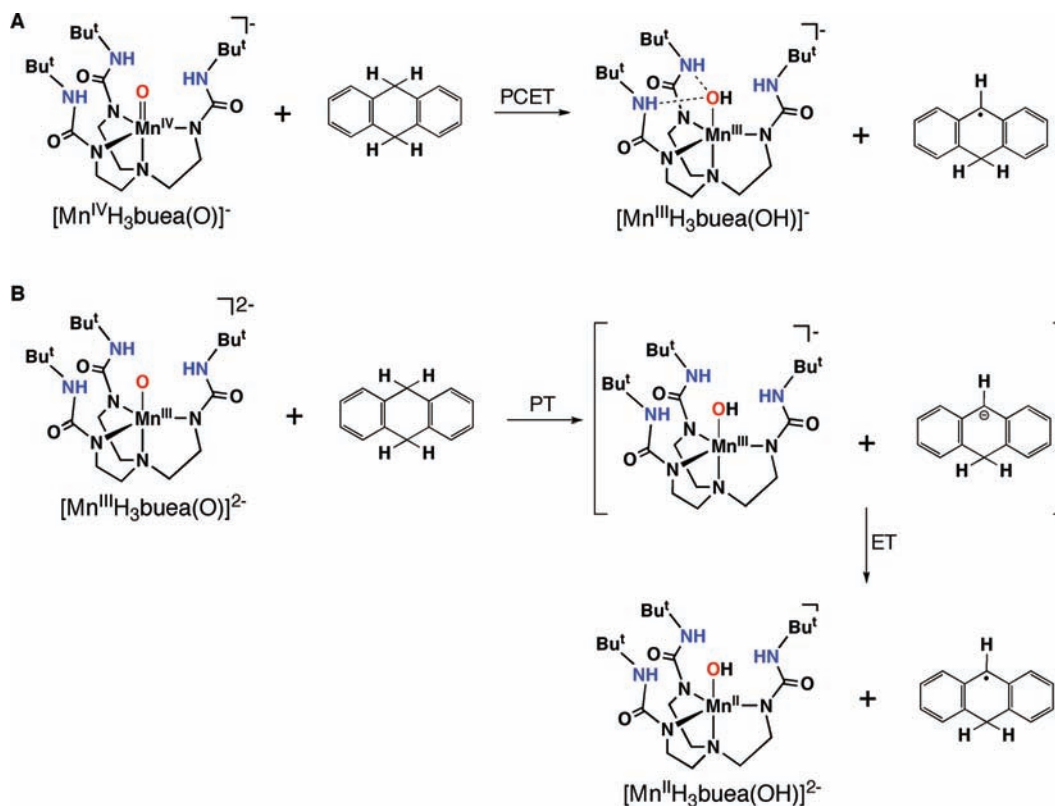


**Figure 20.** Proposed mechanism for the reactions of  $[\text{Mn}^{\text{IV}}\text{H}_3\text{buea}(\text{O})]^-$  and  $[\text{Mn}^{\text{III}}\text{H}_3\text{buea}(\text{O})]^{2-}$  with DHA.

effects of 2.6 and 6.8 found for  $[\text{Mn}^{\text{III}}\text{H}_3\text{buea}(\text{O})]^{2-}$  and  $[\text{Mn}^{\text{IV}}\text{H}_3\text{buea}(\text{O})]^-$ , respectively. These values indicate that both complexes have primary kinetic isotope effects, yet the large disparity in their values suggested the possibility that the complexes might react via different mechanistic paths. This premise was supported by Eyring analysis, which found a 35 eu difference in the entropy of activation between the two complexes ( $\Delta S^\ddagger = -14(6)$  eu for  $[\text{Mn}^{\text{III}}\text{H}_3\text{buea}(\text{O})]^{2-}$  and  $\Delta S^\ddagger = -49(4)$  eu for  $[\text{Mn}^{\text{IV}}\text{H}_3\text{buea}(\text{O})]^-$ ), which had a dominant effect on the rate constants for C–H bond cleavage.

We proposed a mechanistic explanation for the above rate data. Our kinetic finding, coupled with the large difference of  $\sim 15$  between  $\text{p}K_a$  values of DHA and  $[\text{Mn}^{\text{IV}}\text{H}_3\text{buea}(\text{OH})]$ , suggested that these reagents react via a proton-coupled electron transfer (PCET) path (Figure 20A).<sup>60</sup> This mechanism involves the coming together of the substrate and  $\text{Mn}^{\text{IV}}\text{–O}$  complex to form a highly ordered transition state. For  $[\text{Mn}^{\text{III}}\text{H}_3\text{buea}(\text{O})]^{2-}$ , the basicity of the oxo ligand influenced the reaction to such an extent that a two-step mechanism occurs, in which proton transfer precedes electron transfer. Moreover, the similar  $\text{p}K_a$  values for  $[\text{Mn}^{\text{III}}\text{H}_3\text{buea}(\text{OH})]^-$  and DHA ( $\Delta\text{p}K_a$  less than 2) and the primary kinetic isotope effect suggested rate-limiting proton transfer. This mechanistic proposal would also produce a charge-delocalized transition state, leading to less ordered solvent

molecules, which agree with the more positive  $\Delta S^\ddagger$  value determined for this reaction (Figure 20B).

The mechanistic findings for these two manganese–oxo complexes highlight the contributions of the  $\text{p}K_a$  (i.e., oxo ligand basicity) on chemical reactivity. Our finding that the rate of C–H homolysis is affected by oxo basicity shows that there is another tunable parameter (other than the redox potential) that can be used in the development of efficient and durable oxidation catalysts. Furthermore, this concept may help resolve a longstanding issue in biochemistry. The evolutionary benefit of coupling  $\text{O}_2$  activation with C–H bond cleavage is well recognized and has been cited as a major factor for the success of aerobic life. However, dioxygen-derived, metal-containing species, especially high-valent metal–oxo species, exist long enough to do irreversible oxidative damage to a protein active site. One means to prevent such detrimental processes is to couple the redox potentials of the metal–oxo species with the basicity of the oxo ligand. The benefit of this effect is shown graphically (Figure 21) for the homolytic cleavage of the C–H bond in methane ( $\text{BDE}_{\text{CH}} = 104$  kcal/mol). At low  $\text{p}K_a$  values, the redox potentials needed to perform this reaction are too high to sustain function. The metal–oxo center would certainly attack other species within the active sites, such as the side chains of amino acids. As the  $\text{p}K_a$  value increases, there is a concomitant lowering of the redox potential of the metal–oxo species to values that ultimately are compatible with a protein. It is the interplay between these two fundamental properties that may lead to the efficient oxidation of substrates within an oxygenase.

(60) There have been several discussions in the literature on the proper nomenclature for this process: two of the most common are H-atom transfer and PCET. We chose to use the latter in this Forum Article. For more detailed discussions, see ref 55b and: Huynh, M. H. V.; Meyer, T. J. *Chem. Rev.* **2007**, *107*, 5004–5064.

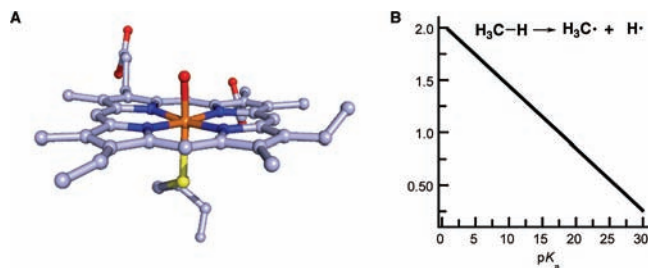


**Figure 21.** Proposed structure of compound I in cytochrome P450 (A) and the relationship between the redox potential and  $pK_a$  for a metal-oxo species in the cleavage of a C-H bond in methane with  $BDE_{C-H} = 104$  kcal/mol (B).

Green was the first to suggest the importance of the basicity of the oxo ligand in oxygenases.<sup>61</sup> They have been exploring the intermediates formed during turnover in P450 compounds and proposed that the redox potentials of the metal-oxo intermediates are much lower than previously thought, thus limiting oxidative damage. In his model, the lower redox potential in compound I, the competent oxidizing species in P450 compounds (Figure 21), is compensated for by the basicity of the oxo ligand in compound II, the one-electron-reduced form of compound I. Green further proposed that this type of chemistry is possible because of thiolate ligation to the iron center, which is supported by resonance Raman studies. Our work described above supports this idea, as do two recent reports on synthetic manganese-oxo<sup>62</sup> and iron-oxo<sup>63</sup> systems.

## Summary

It has been nearly 100 years since Werner first proposed the significance of the secondary coordination sphere in transition-metal complexes. Unbeknownst to Werner were many of the central components that define and control the chemistry associated with this sphere. Some advances have been made in determining the regulatory features for the secondary coordination sphere, as highlighted in this Forum Article. We know that secondary coordination spheres are essential for the function of nearly all metalloproteins and that similar characteristics can be designed into synthetic metal complexes. Its importance is now obvious in the chemistry associated with dioxygen binding and activation, as illustrated with respiratory proteins, oxygenases, and synthetic complexes. Yet, with all of the progress that has been made, our utilization of the secondary coordination sphere still lags far behind that of the primary sphere, in large part because of our inability to manipulate the noncovalent interactions that are needed within the secondary sphere. Examples from our group and others showed that the design of systems with rigid scaffolds allows the positioning of functional groups to promote the formation of intramolecular H bonds while at the same time isolating metal centers in a manner similar to what occurs within a protein active site. These principles should be applicable to most chemical systems using transition-metal ions and undoubtedly

would be beneficial to the development of new or improved function.

## Experimental Section

**General Methods.** All reagents were purchased from commercial sources and used as received, unless otherwise noted. Solvents were sparged with argon and dried over columns containing Q-5 and molecular sieves. Potassium hydride (KH), as a 30% dispersion in mineral oil, was filtered with a medium-porosity glass frit and washed five times each with pentane and Et<sub>2</sub>O. The solid KH was dried under vacuum and stored under an inert atmosphere. 1,2-Diphenylhydrazine (DPH) was recrystallized from Et<sub>2</sub>O, dried under vacuum, and stored under an inert atmosphere. <sup>18</sup>O<sub>2</sub> (99 atom % <sup>18</sup>O) was purchased from ICON Isotopes (Summit, NJ). Elemental analysis was accomplished at Robertson Microлит Laboratories (Madison, NJ). The syntheses of H<sub>3</sub>bpaa and its intermediates were carried out under a dinitrogen atmosphere. The syntheses of metal complexes were conducted in a Vacuum Atmospheres, Co., drybox under an argon atmosphere. *N*-[6-(Bromomethyl)-2-pyridyl]pivalamide<sup>64</sup> was prepared according to literature methods with minor variations.

**Preparative Methods. *N*-(4-Fluorophenyl)-2-bromoacetamide.** A solution of 4-fluoroaniline (5.00 mL, 52.1 mmol) and Et<sub>3</sub>N (8.5 mL, 61 mmol) in 50 mL of CH<sub>2</sub>Cl<sub>2</sub> was cooled to 0 °C with an ice water bath. Bromoacetyl bromide (4.60 mL, 53.0 mmol) was diluted with CH<sub>2</sub>Cl<sub>2</sub> (~50 mL) and added dropwise. The solution was brought to room temperature and stirred overnight. The solution was concentrated under reduced pressure to a solid, dissolved in CHCl<sub>3</sub>, and washed with 2 M HCl (3 × 50 mL), H<sub>2</sub>O (1 × 50 mL), and brine (1 × 50 mL). The organic layer was dried over anhydrous sodium sulfate, filtered, and concentrated to a solid under reduced pressure. The solid was triturated with CH<sub>2</sub>Cl<sub>2</sub> and dried under vacuum to afford 8.06 g (67%). Mp: 132–134 °C. <sup>1</sup>H NMR (500 MHz, CDCl<sub>3</sub>): δ 8.14 (1H, s, NH), 7.50 (2H, m, ArH), 7.06 (2H, m, ArH), 4.03 (2H, s, CH<sub>2</sub>). <sup>13</sup>C NMR (500 MHz, CDCl<sub>3</sub>): δ 164.7, 159.2, 157.3, 135.0, 121.0, 115.6, 115.4, 30.3. <sup>19</sup>F NMR (400 MHz, CDCl<sub>3</sub>): δ 118.8.

**Bis[*N*-[6-pivalamido-2-(pyridylmethyl)benzyl]amine].** A solution of *N*-[6-(bromomethyl)-2-pyridyl]pivalamide (6.11 g, 22.5 mmol), benzylamine (1.2 mL, 11 mmol), and Et<sub>3</sub>N (3.5 mL, 25 mmol) in 100 mL of THF was refluxed for 63 h. The solution was cooled to room temperature, filtered, and concentrated under reduced pressure to a yellow oil. The product was purified by silica gel column chromatography using 2:3 hexanes/EtOAc to yield 4.06 g (76%). Mp: 97–106 °C. <sup>1</sup>H NMR (500 MHz, CDCl<sub>3</sub>): δ 8.10 (2H, d, *J* = 8.3 Hz, NHArH), 7.98 (2H, s, NH), 7.68 (2H, t, *J* = 7.9 Hz, NHArH), 7.39 (2H, d, *J* = 7.5 Hz, NHArH), 7.32 (4H, m, ArH), 7.24 (1H, m, ArH), 3.68 (4H, s, NHArCH<sub>2</sub>), 3.67 (2H, s, NCH<sub>2</sub>Ar), 1.32 (18H, s, C(CH<sub>3</sub>)<sub>3</sub>). <sup>13</sup>C NMR (500 MHz, DMSO): δ 177.5, 158.4, 152.0, 139.1, 139.0, 129.1, 128.8, 127.5, 117.8, 112.9, 59.3, 58.2, 39.8, 27.4.

**Bis[*N*-[6-pivalamido-2-(pyridylmethyl)benzyl]amine].** To a solution of bis[*N*-[6-pivalamido-2-(pyridylmethyl)benzyl]amine (5.54 g, 11.4 mmol) and cyclohexene (33.0 mL, 326 mmol) in 80 mL of EtOH was added 20% Pd/C (0.284 g). The suspension was refluxed overnight, cooled to room temperature, and filtered through a pad of Celite. The filtrate was concentrated under reduced pressure to a yellow solid, washed with Et<sub>2</sub>O, and then dried under vacuum to afford 2.54 g (69%). Mp: 127–128 °C. <sup>1</sup>H NMR (500 MHz, CDCl<sub>3</sub>): δ 8.13 (2H, d, *J* = 8.3 Hz, ArH), 7.99 (2H, s, NHAr), 7.87 (2H, t, *J* = 7.9 Hz, ArH), 7.04 (2H, d, *J* = 7.5 Hz, ArH), 3.86 (4H, s, ArCH<sub>2</sub>), 1.33 (18H, s, C(CH<sub>3</sub>)<sub>3</sub>). <sup>13</sup>C NMR (500 MHz, CDCl<sub>3</sub>): δ 177.1, 157.8, 151.3, 138.8, 118.2, 112.1, 54.3, 39.9, 27.6.

(61) (a) Green, M. T.; Dawson, J. H.; Gray, H. B. *Science* **2004**, *304*, 1653–165. (b) Green, M. T. *Curr. Opin. Chem. Biol.* **2009**, *13*, 84–88.

(62) Lansky, D. E.; Goldberg, D. P. *Inorg. Chem.* **2006**, *45*, 5119–5125.

(63) Sastri, C. V.; Lee, J.; Oh, K.; Lee, Y. J.; Lee, J.; Jackson, T. A.; Ray, K.; Hirao, H.; Shin, W.; Halfen, J. A.; Kim, J.; Que, L., Jr.; Shaik, S.; Nam, W. *Proc. Natl. Acad. Sci. U.S.A.* **2007**, *104*, 19181–19186.

(64) Harata, M.; Hasegawa, K.; Jitsukawa, K.; Masuda, H.; Einaga, H. *Bull. Chem. Soc., Jpn.* **1998**, *71*, 1031–1038.

*N*-[Bis(6-pivalamido-2-pyridylmethyl)](*N'*-4-fluorophenylcarbamoylmethyl)amine (**H<sub>3</sub>bpaa**). A mixture of bis[*N*-(6-pivalamido-2-pyridylmethyl)]amine (3.82 g, 9.61 mmol), *N*-(4-fluorophenyl)-2-bromoacetamide (2.23 g, 9.61 mmol), and Et<sub>3</sub>N (1.4 mL, 10.0 mmol) in 90 mL of THF was refluxed overnight. The reaction mixture was allowed to cool to room temperature, and the Et<sub>3</sub>N·HBr that precipitated from the reaction was removed by filtration. The filtrate was concentrated under reduced pressure to a yellow-orange solid, dissolved in CH<sub>2</sub>Cl<sub>2</sub>, and washed with H<sub>2</sub>O (3 × 100 mL) and brine (1 × 100 mL). The organic layer was dried over anhydrous sodium sulfate, filtered, and concentrated under reduced pressure to a solid. The solid was triturated with Et<sub>2</sub>O and dried under vacuum to afford 4.83 g (92%). Mp: 64–67 °C. <sup>1</sup>H NMR (500 MHz, CDCl<sub>3</sub>): δ 10.12 (1H, s, NHArF), 8.15 (2H, d, *J* = 8.3 Hz, ArH), 7.88 (2H, s, NHAr), 7.66 (2H, t, *J* = 7.9 Hz, ArH), 7.51 (2H, m, HArF), 7.01 (2H, m, HArF), 6.97 (2H, d, *J* = 7.4 Hz, ArH), 3.82 (4H, s, ArCH<sub>2</sub>), 3.51 (2H, s, CH<sub>2</sub>CO), 1.27, (18H, s, C(CH<sub>3</sub>)<sub>3</sub>). <sup>13</sup>C NMR (500 MHz, CDCl<sub>3</sub>): δ 117.1, 169.7, 158.4, 156.0, 151.6, 139.0, 134.1, 121.8, 119.1, 115.8, 112.8, 65.9, 60.0, 58.8, 39.8, 27.5, 15.3. HRMS (ES<sup>+</sup>). Exact mass calcd for C<sub>30</sub>H<sub>37</sub>N<sub>6</sub>O<sub>3</sub>FN<sub>a</sub> [M + Na]: *m/z* 571.2809. Found: *m/z* 571.2797.

*N*-[Bis(6-pivalamido-2-pyridylmethyl)](*N'*-4-fluorophenylcarbamoylmethyl)aminatomanganate(II) ([Mn<sup>II</sup>Hbpaa]). A solution of H<sub>3</sub>bpaa (0.147 g, 0.268 mmol) in 5 mL of anhydrous DMA was treated with solid KH (0.023 g, 0.573 mmol) under an argon atmosphere. The mixture was stirred until H<sub>2</sub> evolution ceased. Mn(OAc)<sub>2</sub> (0.048 g, 0.272 mmol) was added and allowed to stir an additional 45 min. The mixture was filtered to remove KOAc (0.046 g, 88%) to afford 0.159 g (99%) of the pale-yellow product. Mass calcd for C<sub>30</sub>H<sub>34</sub>FN<sub>6</sub>O<sub>3</sub>Mn [M - H]: *m/z* 600.2. Found: *m/z* 600.2. EPR (⊥ mode, X band, 4 K) *g* values: 21.0, 5.6, 3.0, 1.66 1.31.

**Preparation of [Mn<sup>III</sup>H<sub>2</sub>bpaa(O<sub>2</sub>)] via O<sub>2</sub> and DPH.** A solution of [MnHbpaa] (0.114 g, 0.190 mmol) and DPH (0.018 mg, 98 mol) in 4 mL of anhydrous DMA was treated with excess dry O<sub>2</sub> and stirred for 10 min. MS (ES<sup>-</sup>). Mass calcd for C<sub>30</sub>H<sub>35</sub>FN<sub>6</sub>O<sub>3</sub>Mn<sup>16</sup>O<sub>2</sub> [M - H]: *m/z* 633.2. Found: *m/z* 633.2. Mass calcd for C<sub>30</sub>H<sub>35</sub>FN<sub>6</sub>O<sub>3</sub>Mn<sup>18</sup>O<sub>2</sub> [M - H]: *m/z* 637.2. Found: *m/z* 637.1. After treatment with H<sub>2</sub>O (3 mL), the solution was washed with Et<sub>2</sub>O (3 × 3 mL). Concentration of the Et<sub>2</sub>O solution gave 16 mg (89%) of an orange solid. Analysis by <sup>1</sup>H NMR spectroscopy indicated that the solid was azobenzene. Via H<sub>2</sub>O<sub>2</sub>: A solution of [MnHbpaa] (57 mg,

95 μmol) in 3 mL of anhydrous DMSO was treated with H<sub>2</sub>O<sub>2</sub> (6 μL, 160 μmol, 71.2% aqueous) and stirred for 5 min. MS (ES<sup>-</sup>). Mass calcd for C<sub>30</sub>H<sub>35</sub>FN<sub>6</sub>O<sub>5</sub>Mn [M - H]: *m/z* 633.2. Found: *m/z* 633.2. λ<sub>max</sub> [DMSO, nm (ε, M<sup>-1</sup> cm<sup>-1</sup>)]: 590, 460 (sh).

**Reaction of [Mn<sup>III</sup>Hbpaa(O<sub>2</sub>)] with Cyclohexanecarboxaldehyde.** [Mn<sup>III</sup>Hbpaa(O<sub>2</sub>)] was prepared by the method above and allowed to stir for 10 min. A total of 1 equiv of cyclohexanecarboxaldehyde was added via a syringe and allowed to stir an additional 3 h. After treatment with H<sub>2</sub>O (3 mL), the solution was washed with Et<sub>2</sub>O (3 × 3 mL). The Et<sub>2</sub>O washings were combined in a 10 mL volumetric flask and diluted. The solution was analyzed by gas chromatography (GC), and the amount of cyclohexanone was determined from calibration curves.

**Physical Methods.** Electronic absorbance spectra were recorded with a Cary 50 spectrophotometer using a 1.00 mm quartz cuvette. FTIR spectra were collected on a Varian 800 Scimitar series FTIR spectrometer. <sup>1</sup>H and <sup>13</sup>C NMR spectra were recorded on a Bruker DRX500 spectrometer. EPR spectra were collected using a Bruker EMX spectrometer equipped with an ER041XG microwave bridge, an Oxford Instrument liquid-helium quartz cryostat, and a dual-mode cavity (ER4116DM) or a Bruker ESP300 spectrometer equipped with an Oxford ESR910 cryostat and a bimodal cavity (Bruker ER4116DM). MS of the manganese complexes was done on a Waters LCT Premier mass spectrometer operated in negative-ion ESI mode. Identification of the organic products was done on a Thermo Trace MS<sup>+</sup> GC-MS operated in ESI mode. Quantitative GC analysis was done on a Hewlett-Packard 6890 series gas chromatograph equipped with a HP 7683 series injector. A calibration plot was established using standard procedures for the quantitative determination of organic products.

**Acknowledgment.** Acknowledgment is made to the NIH (Grant GM 050781) and the NSF (Grant 0738252) for financial support. We are thankful for the numerous co-workers who have contributed to the work presented here from our laboratory, including C. MacBeth, R. Gupta, T. Parsell, M.-Y. Yang, R. Lucas, M. Zart, M. Hendrich, W. Gunderson, and E. Solomon.

**Supporting Information Available:** CIF for the X-ray experiment on [Mn<sup>II</sup>Hbpaa]. This material is available free of charge via the Internet at <http://pubs.acs.org>.